ELSEVIER

Nickel-based rechargeable batteries

A.K. Shukla[a,*], S. Venugopalan[b], B. Hariprakash[a]

[a]*Solid-state and Structural Chemistry Unit, Indian Institute of Science, Bangalore 560012, India*
[b]*Battery Division, Power Systems Group, ISRO Satellite Centre, Bangalore 560017, India*

Abstract

Nickel–iron (Ni–Fe), nickel–cadmium (Ni–Cd), nickel–hydrogen (Ni–H$_2$), nickel–metal hydride (Ni–MH) and nickel–zinc (Ni–Zn) batteries employ nickel oxide electrodes as the positive plates, and are hence, categorised as nickel-based batteries. This article highlights the operating principles and advances made in these battery systems during the recent years. In particular, significant improvements have been made in the Ni–MH batteries which are slowly capturing the market occupied by the ubiquitous Ni–Cd batteries. © 2001 Elsevier Science B.V. All rights reserved.
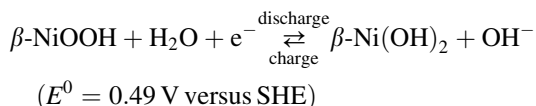
Keywords: Nickel-based rechargeable batteries; Sodium–nickel chloride batteries; Zebra batteries; Bode diagram

1. Introduction

The charge–discharge reactions of the nickel electrode have been expressed as [1]

$$NiO_2 + 2H_2O + 2e^- \underset{charge}{\overset{discharge}{\rightleftarrows}} Ni(OH)_2 + 2OH^-$$

$$(E^0 = 0.49 \text{ V versus SHE}) \tag{1}$$
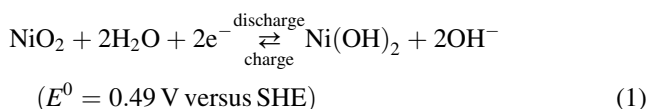
In Eq. (1), NiO$_2$ forms the active material of the positive plate with Ni(OH)$_2$ as the discharged product which is reconstituted as NiO$_2$ during recharge. In practice, β-Ni(OH)$_2$ is the discharged product and this is reconstituted as β-NiOOH during recharge. Accordingly, Eq. (1) is better expressed as

$$\beta\text{-NiOOH} + H_2O + e^- \underset{charge}{\overset{discharge}{\rightleftarrows}} \beta\text{-Ni(OH)}_2 + OH^-$$

$$(E^0 = 0.49 \text{ V versus SHE})$$

The reversible electrode potential (E_{rev}) for the nickel positive electrode is expressed by the Nernst relationship as

$$E_{rev} = 0.49 - 0.059 \log\left(\frac{a_{[Ni(OH)_2]}a_{[OH^-]}}{a_{[NiOOH]}a_{[H_2O]}}\right) \tag{3}$$

In the light of the paper by Corrigan and Knight [2], it is appropriate to express β-Ni(OH)$_2$ as H$_2$NiO$_2$ and β-NiOOH as HNiO$_2$, both of which can be expressed by the general formula: H$_x$NiO$_2$, where $x = 2$ refers to β-Ni(OH)$_2$ and

$x = 1$ to β-NiOOH. The oxidation state of nickel is +2 in β-Ni(OH)$_2$ and +3 in β-NiOOH. On prolonged charging, β-NiOOH transforms irreversibly to γ-NiOOH, where the oxidation state of nickel is found to be +3.7, which corresponds to a formula of H$_{0.3}$NiO$_2$. The mechanism of the reaction shown by Eq. (2) involves an equivalent diffusion of hydrogen ions (protons) through the solid-state lattices of β-Ni(OH)$_2$ and β-NiOOH such that there is a continuous change in the composition of the active material between the fully-charged β-NiOOH and fully-discharged β-Ni(OH)$_2$. Accordingly, Eq. (2) may as well be written as

$$\beta\text{-NiOOH} + H^+ + e^- \underset{charge}{\overset{discharge}{\rightleftarrows}} \beta\text{-Ni(OH)}_2 \tag{4}$$
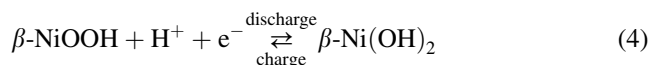
As shown in the Bode diagram (Fig. 1), γ-NiOOH is electrochemically reversible with α-Ni(OH)$_2$. Since a larger number of electrons are exchanged per nickel atom during the α ⇔ γ phase transition, a higher theoretical capacity is expected for a nickel positive electrode comprising α-Ni(OH)$_2$ than β-Ni(OH)$_2$. However, in an alkaline medium, α-Ni(OH)$_2$ transforms to β-Ni(OH)$_2$ on ageing. Efforts [3] are therefore, being expended to synthesise alkali-stable α-Ni(OH)$_2$ which has a turbostatic layered-structure with an interlayer spacing of ca. 8 Å along its *c*-axis as against interlayer spacing of only 4.6 Å along the *c*-axis for the β-Ni(OH)$_2$ (Fig. 2).

The low solubility-product ($K_{sp} = 10^{-35}$) of nickel hydroxide provides excellent stability to it in an alkaline medium. Although the solubility of Ni(OH)$_2$ active material in concentrated potassium hydroxide solutions is significantly low, it cannot be ignored. In a recent publication,

* Corresponding author. Tel.: +91-80-309-2795; fax: +91-80-360-1310.
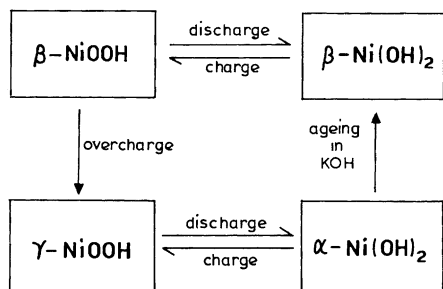*E-mail address*: shukla@sscu.iisc.ernet.in (A.K. Shukla).

Fig. 1. Bode diagram showing the transformations among various phases of nickel positive electrode.

Thaller and Zimmerman [4] has shown that the charge efficiency of the nickel electrode stored in the discharged state can be considerably lower due to Ostwald ripening [5], a process where thermodynamic stability is achieved by reduction in the surface-area of crystallites of β-Ni(OH)$_2$ through a dissolution–precipitation process in which bigger crystals grow at the expense of smaller crystals. This has been experimentally verified by Borthomieu [6]. However, the process is reversible and the material can be brought back to its original crystal form through repeated charge–discharge cycling.

The nickel electrode involves homogeneous solid-state oxidation of β-Ni(OH)$_2$ to β-NiOOH during its charge and vice versa during its discharge, with an inherently long cycle-life. An ideally-reversible battery requires its electrodes to be of the second kind, in which the active masses at its electrodes form true solid solutions at all states-of-charge values with the electrodes kept in contact with a common electrolyte. There is a natural tendency for crystal growth and consequent phase segregation with many of the battery electrodes of the second kind. Hence, the formation and preservation of homogeneous solid solutions of oxidants and reductants or the prevention of phase segregation at the electrodes may have to be realised using spacing agents isomorphous with their active mass. The nickel oxide electrode employs Co(OH)$_2$ which is isomorphous both with β-NiOOH and β-Ni(OH)$_2$, as the spacing agent [7].

In the beginning, developmental work on large-scale commercial applications of nickel electrodes was based on pocket-plate technology initiated in Sweden, Germany and US during 1897–1903. In pocket-plate technology, the active material is first palle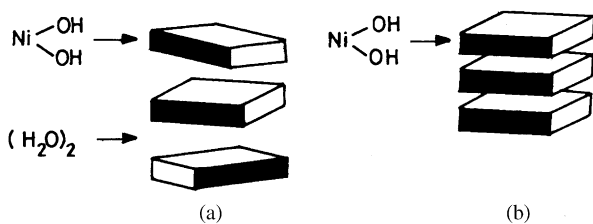tised with a conductive additive and a binder, and the pellets are then wrapped in a perforated nickel-plated steel sheet (pocket) to serve as a current collector and also to provide mechanical support. The next major improvement in nickel electrode structure was the tubular-plate development by Edison in 1908 to restrict the mechanical forces due to swelling of the positive active mass and to extend the cycle-life of the electrodes during deep-discharge cycling applications. In tubular-plate construction, perforated nickel-plated mild steel tubes were filled with alternating layers of nickel hydroxide and nickel flakes/graphite. The active material layers in the tube were compacted as and when they were introduced into the tube. The individual tubes had metal bands spaced at regular intervals along the length of the tube in order to control active material expansion during cycling. The tubes were then crimped at the ends. A number of tubes were arranged in parallel in a frame to form the tubular-plate electrode. Due to the cumbersome manufacturing process and high production cost, the tubular-plate nickel electrodes are no longer being produced [8,9].

Sintered-plate technology is considered as an important milestone in the development of nickel electrodes. The development of sintered-nickel plaques was initiated by Pflider in 1928 [8]. Sintering is defined as a thermal process in which the loose nickel particles are transformed into a coherent body at a temperature just below the melting point of nickel in a reducing atmosphere. More than 50% of batteries based on nickel electrodes being currently manufactured use sintered electrodes for the positive plate. In sintered electrodes, a porous sintered plaque retains the positive active material within the pores and serves to conduct the electric current to and from the active material. Sintered plaques are produced either by a wet-slurry process or by a dry-powder (loose-powder) process. In both these processes, sintered plaques are produced by locating a pure nickel mesh or a perforated nickel-plated steel sheet centrally across the thickness of the carbonyl nickel powder (INCO 287) layer followed by sintering at temperatures between 800 and 1000°C in a reducing atmosphere. Wet-slurry plaques are manufactured by coating on both sides of a nickel-plated steel or nickel grid or other current collecting material uniformly to a desired thickness with a viscous slurry comprising carbonyl nickel powder (INCO 255), a pore former/expander, binder and water, drying the plaques to evaporate the water, and finally sintering them between 800 and 1000°C in a reducing atmosphere. Sintered nickel electrodes have been the dominant technology for several decades in most applications. These consist of a porous nickel plaque of sintered high surface-area nickel particles impregnated with nickel hydroxide active material either by chemical or electrochemical methods. The chemical impregnation of the sintered nickel plaque involves filling the pores with aqueous Ni(NO$_3$)$_2$, cathodically polarising the filled plaque in NaOH solution to convert it to Ni(OH)$_2$, rinsing, drying and weighing. The weight pick-up is a measure of capacity. The process is repeated until the weight pick-up

Fig. 2. Layered-structures in (a) turbostratic α-Ni(OH)$_2$ and (b) β-Ni(OH)$_2$.

meets the required capacity criteria. Electrochemical impregnation of sintered nickel plaque involves cathodic polarisation of the plaque in hot, aqueous or alcoholic solution of $Ni(NO_3)_2$ of pH 3 at a current density between 5 and 75 mA cm^{-2}. The plaques may be passivated before impregnation to avoid corrosion and material build-up on the surface and eventual plate thickening, especially during the aqueous impregnation process. The loose/dry-powder sintering process is exclusively used in the production of hermetically sealed aerospace Ni–Cd and Ni–H_2 cells. The dry-powder process is labour intensive and hence, expensive. The essential features of sintered plaques are high-porosity, large surface-area and high electrical conductivity in combination with good mechanical strength. For commercial applications sintered-plates are produced by a wet-slurry process. Sintered nickel electrodes have a relatively higher inert to active material weight ratio, utilise an excess amount of nickel per ampere hour, involve laborious processing and require a number of effluent streams to avoid environmental pollution. Hence, for large-scale applications, roll-compacted plastic-bonded electrodes are preferred for economical and cost-effective production of nickel electrodes. In plastic-bonded electrodes, a plastic binder is utilised to impart structural integrity to the electrode. For such electrodes to function effectively, the binder must provide sufficient structural integrity to the electrode while maintaining particle to particle contact. Besides, the electrolyte access to active material must not be restricted.

Sintered-nickel electrodes are fabricated either by pressing the active mass with a suitable binder and a conductive additive on to a substrate of inert metal (pressed-plate design) or by using sintered (inert) metal substrate to contain the active mass in its pores. The presence of binder in the pressed-plate design contributes to increased electrode resistance. By contrast, the absence of binder reduces the structural integrity of the electrode. The conductive additive has to form a continuous chain without which the electrode resistance is further increased. In the sintered-plate design, structural integrity is achieved without any binder in the active mass and continuity of the conductive path is accomplished without any particulate additive to the active mass. The sintered-plate configuration is inherently very efficient. The degree of utilisation (Faradic efficiency) of nickel positive electrodes varies from 60% for the pocket/pressed-plate to 90% for the sintered-plate electrodes. The superior performance of the latter is due to the property of the sintered support which acts as a porous electrode as well as a current collector. Introduction of new electrode manufacturing techniques is likely to yield improvements in future. The process of making sintered electrodes is a well established art. Conventional sintered-electrodes normally have a volumetric Coulombic capacity of about 500 Ah l^{-1}. At present, in order to achieve higher loadings, foam and pasted electrodes are being preferred.

Pasted nickel electrodes consist of nickel hydroxide particles in contact with a conductive network or substrate, preferably having a high surface-area. There have been several variants of these electrodes including the plastic-bonded nickel electrodes which utilise graphite as a micro-conductor, and the foam–metal electrodes which utilise high-porosity nickel foam as a substrate loaded with spherical nickel hydroxide particles and cobalt as conductivity-enhancing additive. Indeed, pasted electrodes of the foam–metal type have penetrated the consumer market due to their low cost and higher energy density in relation to sintered nickel electrodes.

Foam nickel electrodes, which were introduced in the mid 1980s, function in a similar fashion to sintered-plate electrodes. A major development at INCO laboratory has been the invention of INCOFOAM^{TM}, a high-porosity nickel substrate [10]. The process involves production of the high-purity nickel foam through single step process using an INCO refinery intermediate gas stream. The excellent throwing power of the gas decomposition results in a uniform nickel density distribution. This unique process allows for the development of nickel foam of different thickness and porosity to suit customer needs. A nickel frame work with approximately 95% free volume is created by nickel plating a porous synthetic material (polyurethane or acrylic fibre) followed by pyrolysis of the plastic material. The utilisation of active material in these electrodes is poorer than in sintered-plates. The higher pore volume and larger active material holding capacity (reduction in conducting substrate weight) more than compensates for the loss of utilisation efficiency and consequently improves the energy density of the cell.

Fibre nickel electrodes were introduced into the market in late 1970s. These electrodes are manufactured by nickel plating a mat of synthetic fibres (graphite or plastic) by an electroless method followed by sintering under compression at 800°C in a hydrogen atmosphere to form mats with 90% free volume and subsequent impregnation with the active mass. Mechanical impregnation is used in all these advanced technology electrodes which allows production of electrodes with a thickness ranging from 0.6 to 10 mm without much variation in the ratio of current conducting substrate to active mass [8].

Nickel oxide electrodes constitute the positive plates of various storage batteries, namely nickel–iron (Ni–Fe), nickel–cadmium (Ni–Cd), nickel–hydrogen (Ni–H_2), nickel–metal hydride (Ni–MH) and nickel–zinc (Ni–Zn) rechargeable batteries. In the following sections, we will discuss the electrochemistry and operating principles of these nickel-based battery systems.

2. Nickel–iron batteries

The Ni–Fe battery was developed by Edison in the USA and Jüngner in Sweden in 1901. The battery is based on the use of nickel oxyhydroxide (NiOOH) at the positive electrode and iron at the negative electrode.

The charge–discharge reactions of the battery are

$$2NiOOH + Fe + 2H_2O \underset{charge}{\overset{discharge}{\rightleftarrows}} 2Ni(OH)_2 + Fe(OH)_2$$
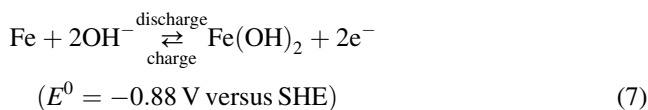
$$(E_{cell} = 1.37 \, V) \tag{5}$$
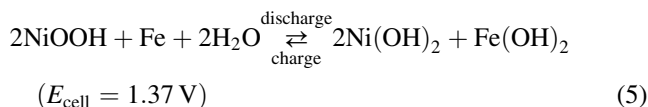
Under deep-discharge, a Ni–Fe cell with a negative-limited configuration will undergo a further discharge reaction at a potential that is lower than the first step represented by reaction (5), i.e.

$$NiOOH + Fe(OH)_2 \underset{charge}{\overset{discharge}{\rightleftarrows}} Ni(OH)_2 + FeOOH$$
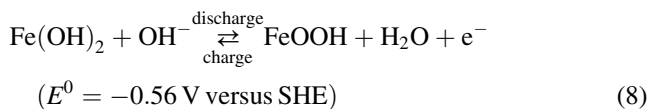
$$(E_{cell} = 1.05 \, V) \tag{6}$$
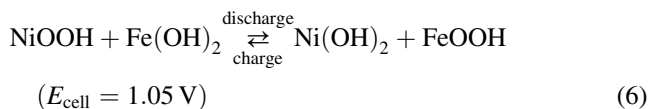
The cell reactions are highly reversible in the alkaline electrolyte, particularly, if the discharge is limited to the first step. The reversibility at the two electrodes confers a long charge–discharge cycle-life of the battery. The two sets of electrodes are arranged alternately and interlaced with porous separators usually of polyvinyl chloride, polyethylene, polyamide or polypropylene. The whole electrode stack is kept immersed in a solution of alkaline electrolyte (30 wt.% aqueous KOH). Cell terminals and links are usually made from nickel-plated mild steel. The cells are provided with vents, which may be of different designs, to prevent spillage and carbonation while permitting the escape of gases produced in the cell. Positive-limited Ni–Fe cells yield better cycle-life [11]. Even under abusive usage that involves mechanical shocks and vibrations, overcharge/overdischarge and storage in a charged or discharged state, the cycle-life of the Ni–Fe battery, with deep-discharge between cycles, is of the order of 3000 cycles and the calendar life is about 20 years [12–18].
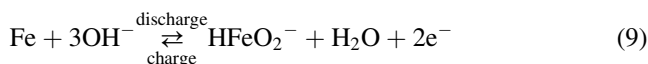
The charge–discharge reactions at the negative electrode of the Ni–Fe cell occur in two steps [13,15,16,19,20] represented as
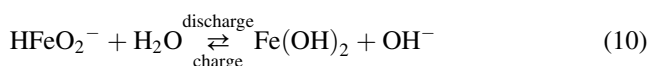
$$Fe + 2OH^- \underset{charge}{\overset{discharge}{\rightleftarrows}} Fe(OH)_2 + 2e^-$$

$$(E^0 = -0.88 \, V \, versus \, SHE) \tag{7}$$

and

$$Fe(OH)_2 + OH^- \underset{charge}{\overset{discharge}{\rightleftarrows}} FeOOH + H_2O + e^-$$

$$(E^0 = -0.56 \, V \, versus \, SHE) \tag{8}$$

The mechanism of electrode reaction (7) involves both solid and liquid phases (heterogeneous mechanism) with $HFeO_2^-$ as the dissolved ion intermediate [20–22] which, on further discharge, converts to $Fe(OH)_2$. Thus, the actual course of the electrode reaction (7) is

$$Fe + 3OH^- \underset{charge}{\overset{discharge}{\rightleftarrows}} HFeO_2^- + H_2O + 2e^- \tag{9}$$

followed by

$$HFeO_2^- + H_2O \underset{charge}{\overset{discharge}{\rightleftarrows}} Fe(OH)_2 + OH^- \tag{10}$$

During prolonged discharge of the iron-electrode, there is a continuous change in the composition of active $Fe(OH)_2$ to δ-FeOOH and, akin to the nickel positive electrode, the mechanism of the electrode reaction involves diffusion of protons between the solid lattices of $Fe(OH)_2$ and δ-FeOOH. As the transformation of $Fe(OH)_2$ to δ-FeOOH is a bulk feature, the mechanism involved during the second discharge step is homogeneous in nature [23].

The open-circuit potential of the charged alkaline iron-electrode is always more cathodic than the hydrogen electrode reaction in the same solution [24]. Consequently, iron is thermodynamically unstable and suffers corrosion through local cells with hydrogen evolution reaction

$$2H_2O + 2e^- \rightarrow H_2 + 2OH^-$$

$$(E^0 = -0.83 \, V \, versus \, SHE) \tag{11}$$
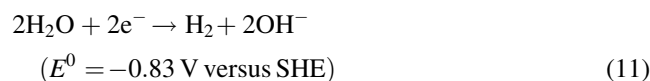
as the conjugate reaction.

Besides, the dissolved oxygen in an alkaline solution can also lead to an oxygen reduction reaction

$$O_2 + 2H_2O + 4e^- \rightarrow 4OH^-$$

$$(E^0 = 0.41 \, V \, versus \, SHE) \tag{12}$$
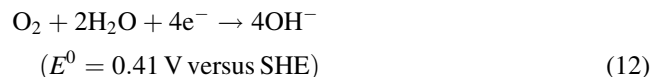
as a conjugate reaction during the corrosion of the iron-electrode.

Owing to these corrosion reactions, the alkaline iron-electrodes undergo a self-discharge of about 1–2% of their nominal capacity per day at 25°C. Hydrogen evolution also occurs concomitantly while charging the alkaline iron-electrodes and brings about a decrease in the charge acceptance. The degree of utilisation (or the Faradaic efficiency) of iron-electrode, based on reaction (7), varies from about 30% for electrodes of commercially pure iron to 60% for electrodes that comprise high-purity iron.

A typical charge–discharge curve of a commercial Ni–Fe cell is shown in Fig. 3, while discharge curves at different rates at 25°C are given in Fig. 4. The data show that the nominal (operating or discharge) voltage of Ni–Fe cells
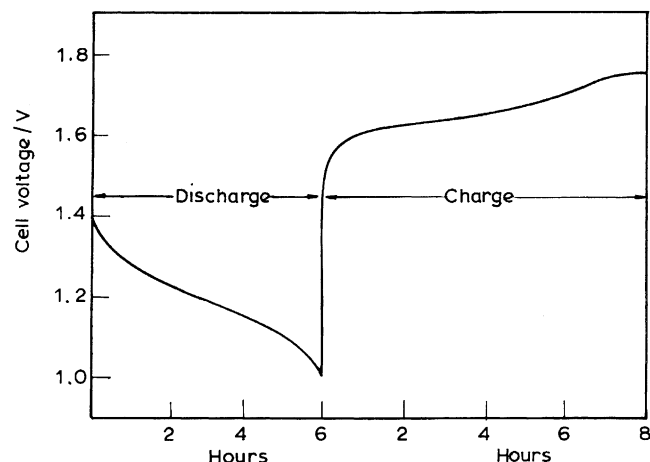

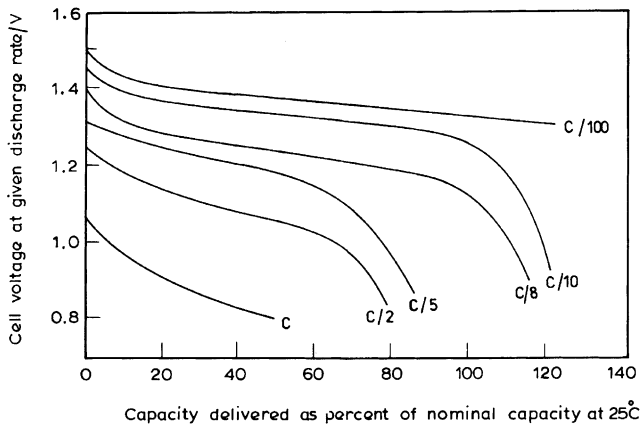
Fig. 3. Typical charge–discharge curves for a Ni–Fe cell.

Fig. 4. Typical discharge curves for a Ni–Fe cell at various rates at 25°C. Numbers on curves are discharge rates with C as the nominal Ah capacity of the cell.

Fig. 6. Discharge capacity of a Ni–Fe cell at end of different periods of storage.

could vary from about 1.23 V at the $C/8$ rate to 0.85 V at the C rate. The open-circuit voltage, as well as the nominal voltage at discharge rates between $C/10$ and $C/100$ is ~1.3 V. The discharge curves are fairly flat with the change in the cell voltage at the $C/8$ rate, i.e. 1.32 V at 10% depth-of-discharge to about 1.15 V at 90% depth-of-discharge. The discharge capacity of the Ni–Fe battery or cell is not only dependent on its discharge rate, but also on the operational temperature as shown in Fig. 5. This limits the application of Ni–Fe batteries for high discharge at low temperatures.

The self-discharge profile of a Ni–Fe cell shown in Fig. 6 indicates that the rate of self-discharge could be as high as 8–10% of the nominal capacity per day at an operational temperature of about 40°C. Therefore, at high ambient temperatures, the Ni–Fe battery is useful only for applications where the duty schedule permits a recharge at least on

every alternate day or so, in order that a minimum of 80% of the nominal capacity be available during discharge. At 20°C and below, the self-discharge rate of the Ni–Fe cell is, however, considerably less. At these operational temperatures, the interval between recharges could be a month or more in order that the battery may be able to deliver at least 80% of its nominal capacity at any point of time.

At operational temperatures <30°C, the charge–discharge cycle-life of Ni–Fe batteries is of the order of 3000 cycles under normal conditions of use in industrial traction vehicles and railway-carriage service that involve deep-discharge between cycles, moderate vibrations, and shocks with fairly regular duty schedules. Under similar conditions of usage, a calendar life of about 20 years has been realised for the Ni–Fe batteries. But at operational temperatures of about 45°C, the service life of the Ni–Fe battery is nearly 1500 charge–discharge cycles with about 8 years of calendar life. The wet shelf-life of Ni–Fe batteries in the discharged state exceeds 2 years. The battery provides the normal charge–discharge cycle-life even after a continuous period of wet storage in its discharged state. The wet shelf-life can be extended to 10 years or more with a reconditioning cycle every 6 months or so. Therefore, even with irregular duty schedules or periods of neglect under field conditions, the actual service life of Ni–Fe batteries remains unaffected. The only routine maintenance operation for batteries in service is the addition of water to make up for the losses during overcharge.

Ni–Fe batteries are usually charged galavanostatically. Charging is usually performed at the $C/5$ rate for 7 h and could go up to $C/3$ for 4 h. The higher charging rates are permissible provided the temperature of the electrolyte at the end-of-discharge does not exceed 45°C. Typical charging curves for a Ni–Fe cell at 25°C are shown in Fig. 7. The
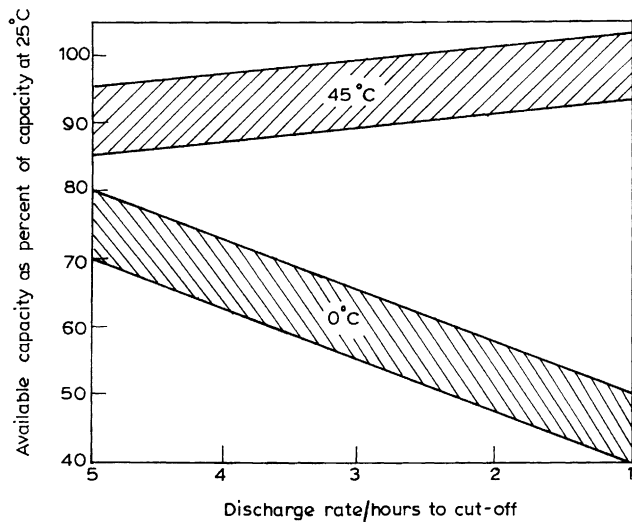

Fig. 5. Discharge capacity at high and low temperatures for a Ni–Fe cell vs. rate of discharge. The band spread shown is due to differences in size, type and number of cells in the battery packs.
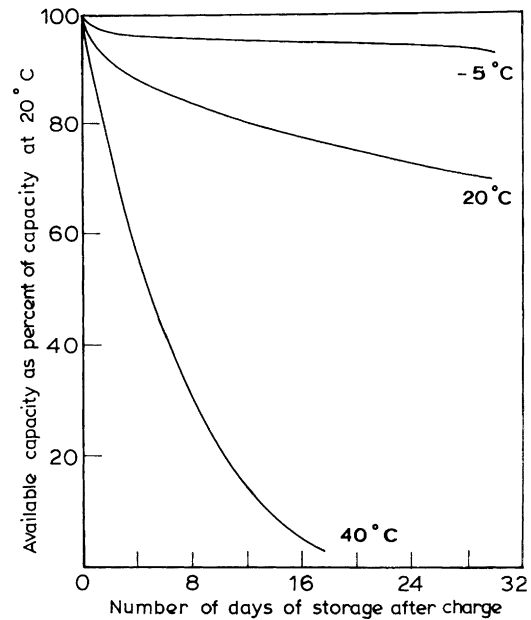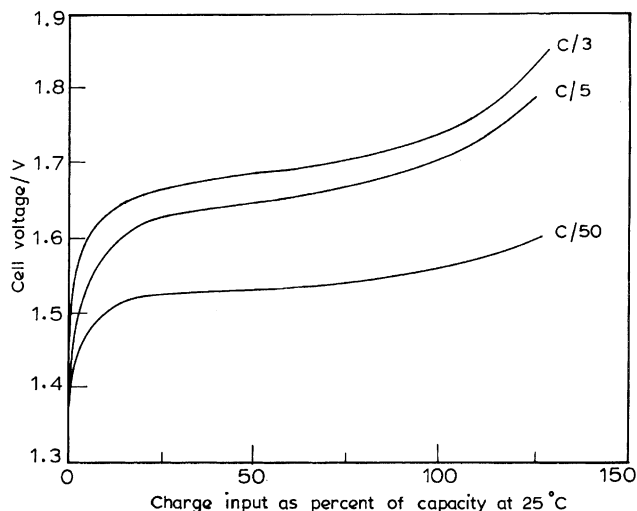
Fig. 7. Typical charging curves for a Ni–Fe cell at 25°C. Numbers on curves are charging rates with C as the nominal capacity of the cell.

average voltage at the normal $C/5$ rate charging is between 1.6 and 1.65 V up to about 50% state-of-charge (SOC). The charging voltage gradually rises to $\sim$1.85 V at the end of full charge.
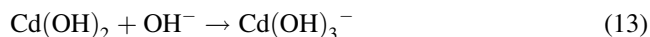
The key problem in the development of Ni–Fe batteries is poisoning of the iron-electrode [25]. As explained above, the iron-electrode undergoes self-discharge as a result of the corrosion reaction. It has been demonstrated that a substantial improvement in the overall performance of Ni–Fe cells is possible by electrocatalysis of the iron-electrode reaction [26,27]. Although a complete suppression of hydrogen evolution appears to be difficult, but if this hydrogen is recombined with evolved oxygen using a hydrogen–oxygen recombinant catalyst [28], then it may be possible to achieve sealed Ni–Fe batteries. This would revive commercial interest in Ni–Fe batteries. Owing to these problems, the iron-electrode in Ni–Fe batteries was replaced with cadmium leading to development of the Ni–Cd system.

3. Nickel–cadmium batteries

Both Jüngner and Edison contributed significantly to the development of the Ni–Cd battery. Initial work on Ni–Cd batteries was limited to pocket-plate technology. Tubular-plate batteries were introduced by Edison in 1908 to restrict the mechanical deformations caused due to swelling of the positive-active mass in pocket-plate batteries and to extend the cycle-life of batteries in deep-discharge cycling applications. Swelling of the positive-active mass was contained by Edison by replacing graphite with nickel flakes as the conductive diluent. However, owing to the cumbersome manufacturing process and high cost of production such tubular-plate batteries are no longer being manufactured.

In a Ni–Cd cell, the charge–discharge reactions at the nickel positive electrode (cathode) proceed via homogeneous solid-state mechanism through proton transfer between nickelous hydroxide (discharged active material) and nickelic hydroxide (charged active material). Cadmium hydroxide is the discharged active material at the negative electrode (anode) of the Ni–Cd cell. During charge, cadmium hydroxide at the negative electrode is converted to metallic cadmium via a dissolved complex intermediate product as described below.

$$Cd(OH)_2 + OH^- \rightarrow Cd(OH)_3^- \qquad (13)$$

$$Cd(OH)_3^- + 2e^- \rightarrow Cd + 3OH^- \qquad (14)$$

The overall reaction at the negative electrode is

$$Cd + 2OH^- \underset{charge}{\overset{discharge}{\rightleftarrows}} Cd(OH)_2 + 2e^-$$

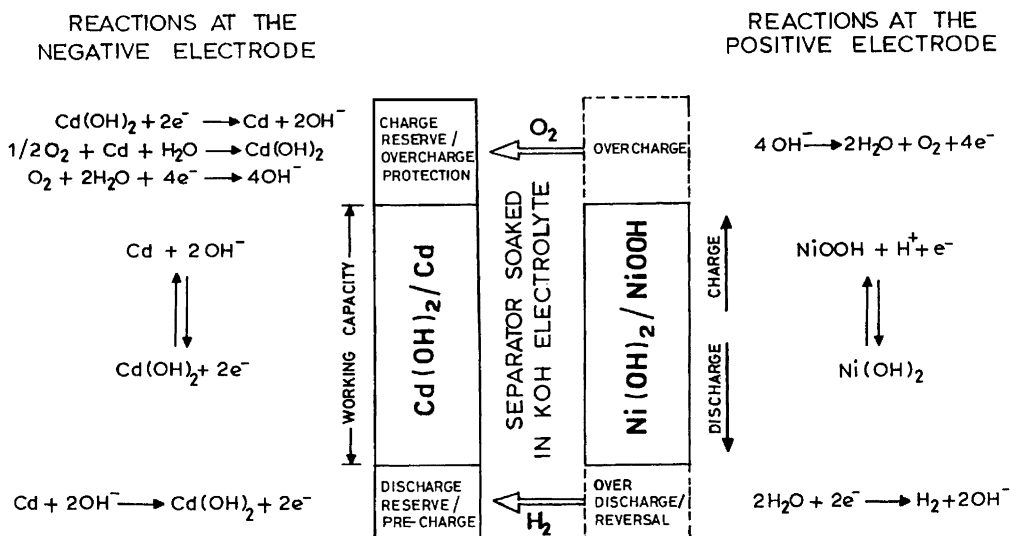$$(E^0 = -0.81V \text{ versus SHE}) \qquad (15)$$
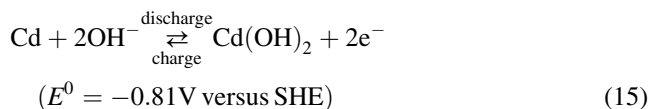
Fig. 8. Operating principle of a sealed Ni–Cd cell.

Accordingly, the overall cell reaction is

$$2NiOOH + Cd + 2H_2O \underset{\text{charge}}{\overset{\text{discharge}}{\rightleftarrows}} 2Ni(OH)_2 + Cd(OH)_2$$

$$(E_{cell} = 1.30\,V) \tag{16}$$
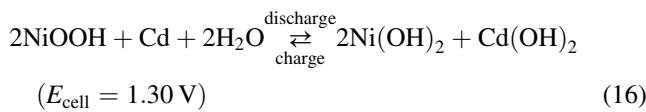
To ensure proper functioning of the sealed Ni–Cd cell under a variety of operating conditions, it is designed to be positive-limited. This insures that only O_2 evolution occurs under normal operating conditions which diffuses to the cadmium electrode and combines with active cadmium to form $Cd(OH)_2$ according to the reaction

$$Cd + \tfrac{1}{2}O_2 + H_2O \rightarrow Cd(OH)_2 \tag{17}$$
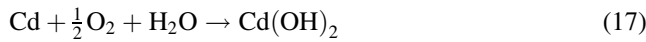
$Cd(OH)_2$ is converted to active Cd according to reaction (15) during the cell charge. The negative to positive plate capacity ratio usually varies between 1.5 and 2. The discharge reserve is typically between 15 and 20% of positive capacity and the charge reserve or overcharge protection is about 30% of positive capacity. Under deep-discharge conditions, due to inevitable differences in storage capacities of series connected cells in the battery, H_2 evolution may occur at the positive electrode which is consumed at a very low rate at the positive electrode. Hence, repeated occurrence of over-discharge may cause internal pressure build-up leading to cell burst. The operating principle of a sealed Ni–Cd cell is depicted in Fig. 8.

The performance of Ni–Cd cells depends on several factors such as cell type, cell construction, manufacturing
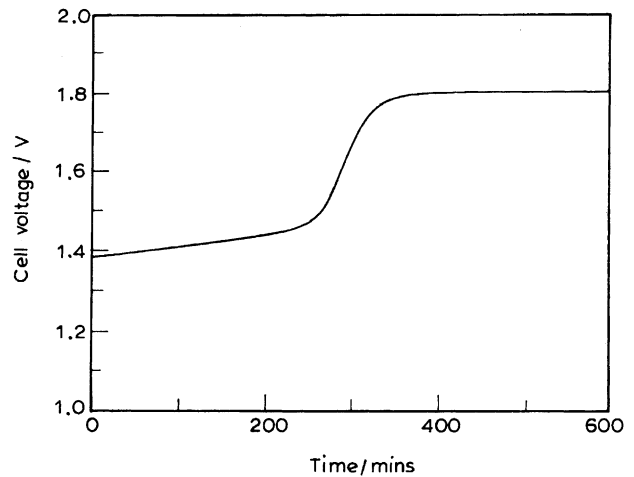
Fig. 9. Charge characteristics of a pocket-plate cell at $C/5$ rate.

process and operating temperature, charge–discharge rates, previous history of the cell, length of open-circuit stand, age of the cells, etc. The typical charge characteristics of a pocket-plate cell at $C/5$ rate at room temperature are shown in Fig. 9. Effect of temperature, rate, cell design and type on the charge characteristics of Ni–Cd cells are shown in Fig. 10. The voltage, temperature and pressure variations during charge of a sealed Ni–Cd cell are shown in Fig. 11. The effect of temperature and rate on the discharge characteristics of the sealed Ni–Cd cells are shown in Fig. 12. The available capacity as a function of temperature and
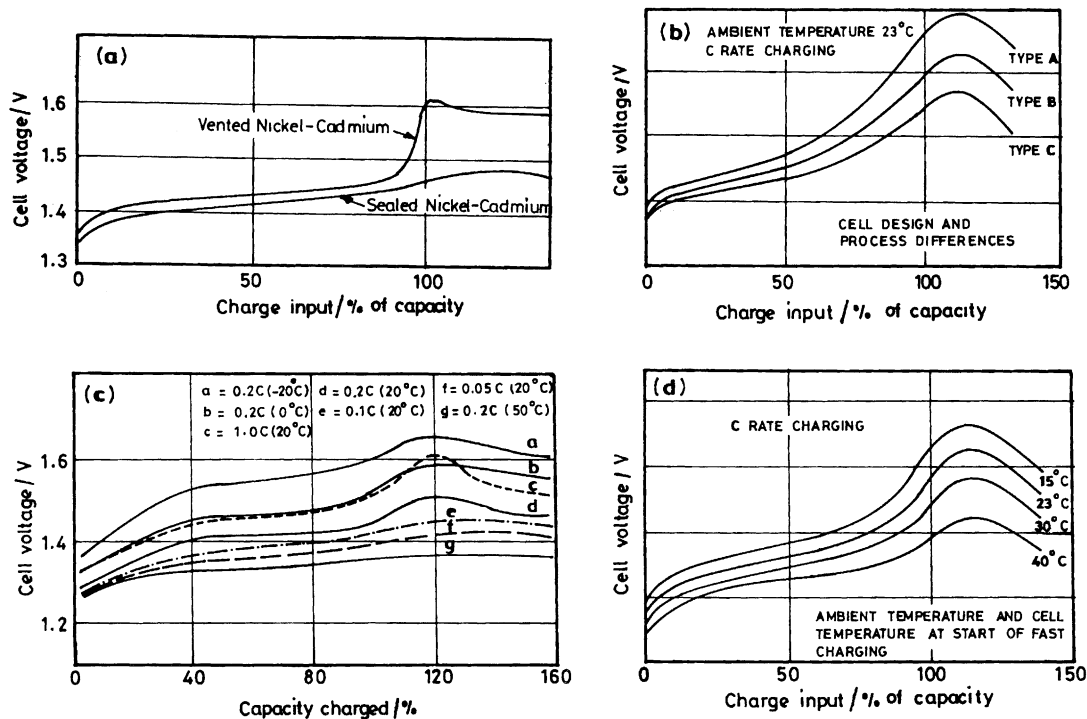
Fig. 10. (a) Charge voltage profiles for different types of Ni–Cd battery at $C/10$ rate; (b) effect of cell design differences on voltage profile of different Ni–Cd cell types; (c) charge curves for a typical sealed Ni–Cd cell at various rates and temperatures, and (d) effect of charge temperature on voltage profile of Ni–Cd cells.
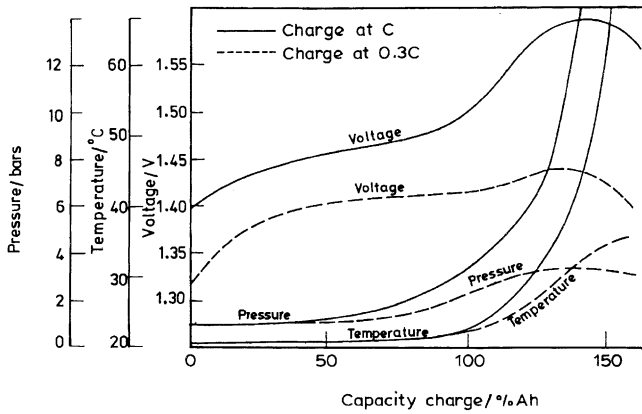
Fig. 11. Voltage, temperature and pressure curves for constant-current charge of a sealed Ni–Cd cell.

discharge rate is shown in Fig. 13. A typical voltage profile on polarity reversal of the Ni–Cd cell is shown in Fig. 14 and the individual electrode characteristics are shown in Fig. 15. The charge retention characteristics of the Ni–Cd cell are depicted in Fig. 16.

The open-circuit voltage of the Ni–Cd cells is independent of KOH concentration between 20 and 30%. In practice, little change occurs in the amount of water especially in vented/flooded electrolyte Ni–Cd cells. In hermetically sealed starved electrolyte cells, formation of water during charge at the positive electrodes causes dilution of electrolyte in the pores of the positive plate active material and in the immediate vicinity of the electrode bringing about a voltage drop or an overvoltage. During high-rate charge–discharge at low temperatures, dilution of electrolyte in pores of one electrode leads to freezing while an increase in electrolyte concentration at the opposite electrode results in precipitation of solid in its pores.

Several authors [29–31] have investigated the effect of foreign cations on the performance characteristics of the nickel active material and its electrical conductivity. For instance, cadmium inhibits electrode swelling and formation of γ-NiOOH, facilitates good charge acceptance at elevated
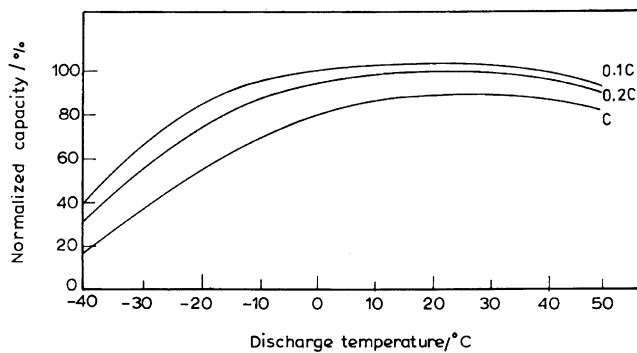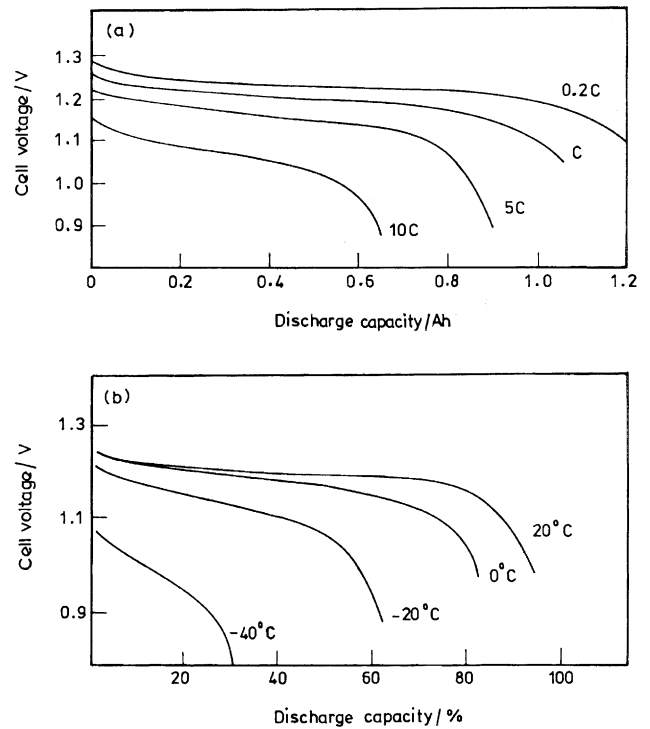

Fig. 13. (a) Discharge curves for a typical 1.2 Ah sealed Ni–Cd cell at various discharge rates; (b) discharge curves for a typical sealed Ni–Cd cell at various temperatures at $C/2$ rate.

temperatures in addition to good stability during cycling and increases the overvoltage for O_2 evolution. Zinc inhibits electrode swelling and formation of γ-NiOOH and increases the overvoltage for O_2 evolution. Lithium eliminates the poisoning effect of iron and increases the overvoltage for O_2 evolution. Iron decreases the overpotential for O_2 evolution, and hence, the electrode capacity. Arsenic acts as the best inhibitor for loss of charge. Cobalt increases the charge efficiency at high-temperature, inhibits loss of charge under open-circuit storage, prevents electrode swelling and formation of γ-NiOOH, minimises number of formation cycles, eliminates the second plateau in plastic-bonded electrodes, increases the overvoltage for O_2 evolution, maximises the

Fig. 12. Effect of discharge rate and temperature on the typical sealed Ni–Cd cell capacity after charge at 20°C.
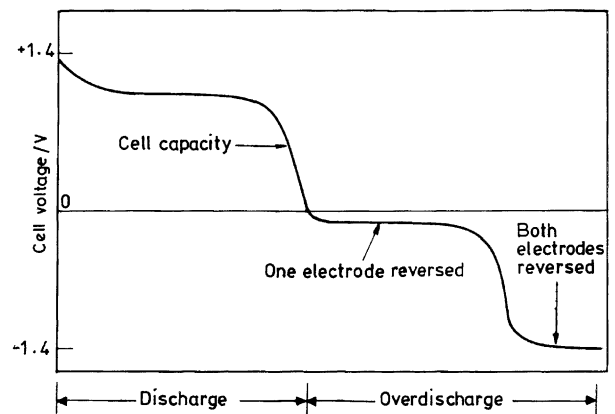

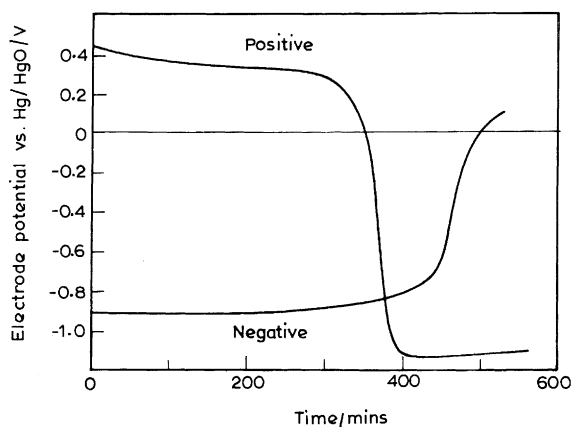Fig. 14. Ni–Cd cell polarity reversal voltages.

Fig. 15. Discharge characteristics at $C/5$ rate of positive and negative plates in a pocket-plate Ni–Cd cell.

oxidation of nickel and increases the reversibility of Ni(II)/Ni(III) reaction and cycle-life stability.

Due to the dissolution–precipitation mechanism at the cadmium electrode, the active mass in the electrode continuously changes on a microscopic scale. Depending on the charge–discharge conditions, the intermediate products migrate within the electrode. The amount, size, form and the location where Cd and $Cd(OH)_2$ crystals grow in an electrode have a significant effect on the electrochemical behaviour of the battery. The cycle-life of the cell depends on the temperature at which charge–discharge cycles are carried out. Low charge–discharge currents and high-temperatures lead to the formation of large crystals of negative active material adversely affecting charge acceptance, energy storage and the discharge capacity of the electrodes. High charge–discharge rates, low operating and storage temperatures, and storage in discharged condition minimise the growth of metallic cadmium and cadmium hydroxide elevating the electrochemical behaviour of the negative electrode.

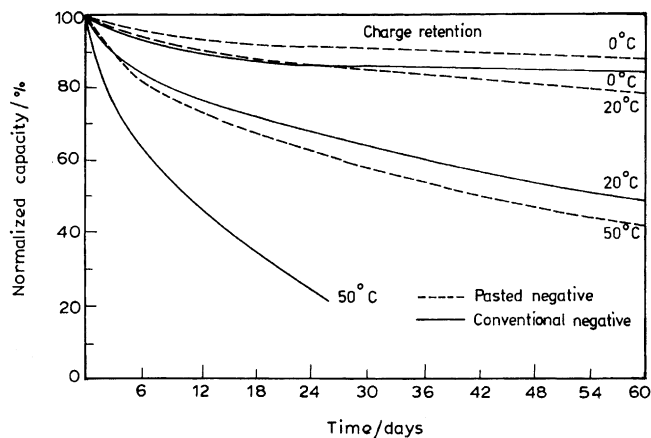The temperature coefficients of cadmium and nickel electrodes are -1.01 and $-0.50\,\mathrm{mV\,K^{-1}}$, respectively.

Fig. 16. Charge retention curves for a sealed Ni–Cd cell at various temperatures.

The temperature coefficient of the Ni–Cd cell is $-0.51\,\mathrm{mV\,K^{-1}}$. The potential of the Cd electrode is invariant with the state-of-charge (SOC), but the Ni electrode potential changes continuously (about 100 mV between 20 and 80% SOC) with its SOC. The exchange current density of the Cd electrode is $7 \times 10^{-7}\,\mathrm{A\,cm^{-2}}$ of geometrical surface-area. There are three different forms of $Cd(OH)_2$, namely α, β and γ. Among these, β-$Cd(OH)_2$ is the most stable phase with one molecule per unit cell. The γ-phase has four molecules per unit cell and dominates at low temperature. It is more active than the β-phase and is more easily charged. The α-phase is poorly crystalline and has the brucite structure. It is the only phase that contains water. It is unstable in KOH and converts to β-$Cd(OH)_2$. Perfectly crystalline stoichiometric β-$Cd(OH)_2$ is electrochemically inactive. Indium is added to the cadmium electrode to make it more active. Choking (clogging of pores) causes mass-transfer limitation whereby the inner part of the electrode ceases to participate in the charge–discharge process. Agglomeration is the gradual accumulation of metallic cadmium into clusters which reduces the available surface-area. When Ni–Cd cells begin to exhibit capacity fading, tests using reference electrodes frequently show problems with the cadmium electrode. Anti-agglomerants are added to limit the Cd metal grain growth which minimises loss of capacity, but improves the operating voltage. The anti-agglomerants work as expanders, favour formation of α-$Cd(OH)_2$, provide protective colloid action, get attached to highly active sites, form complexing reaction with Cd, reduce size of crystals formed, and enhance the dissolution–precipitation process. Some of the anti-agglomerants are carboxy-methyl cellulose, ethyl cellulose, cetyl-trimethyl ammonium bromide, iron, nickel, hydroxy-ethyl cellulose, sodium laural sulphate, sulphonated castor oil, sunflower oil, carbon and polyvinyl alcohol.

The overpotential for H_2 evolution on Cd is between 0.5 and 0.8 V. But Nickel has very low overvoltage for H_2 evolution. From H_2 evolution considerations, sintered-plate electrodes are not as useful as pocket-plate or pasted/roll-compacted electrodes which do not contain metallic nickel. Vented Ni–Cd cells that do not contain nickel at the Cd electrode are likely to have very low water consumption. H_2 evolution in sealed Ni–Cd cells should be eliminated. H_2 reduction can occur at the nickel oxide electrode, but is a slow process. H_2 can diffuse through plastic and metallic materials which could also affect the SOC of the cell.

The typical discharge curves at various stages of cycling for a sealed Ni–Cd cell are depicted in Fig. 17. The shape of the discharge curve changes appreciably on cycling. The discharge profile at the beginning of life is flat, but after cycling appears to have a distinct slope due to possible formation of different phases of nickel oxyhydroxide during extensive cycling or continuous overcharge. The charged and discharged forms of the positive active material exist in multiple phases. During normal charge–discharge cycling of
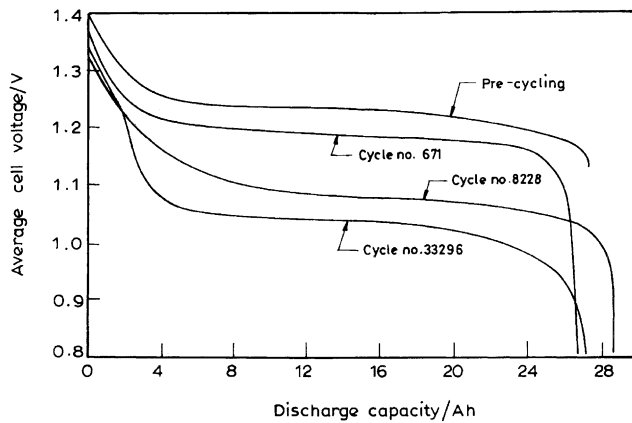
Fig. 17. Typical discharge curves at various stages of cycling for a sealed Ni–Cd cell.

Fig. 18. Oxygen recombination structure in fibre-structured Ni–Cd cells.

chemically prepared active material, β-Ni(OH)$_2$ is converted to β-NiOOH on charge and vice versa on discharge. On prolonged charging or on overcharge, β-NiOOH is converted to γ-NiOOH.

During 1992–1993, SAFT introduced a new range of ultra-low maintenance (ULM) Ni–Cd batteries for aircrafts to limit the penetration of the sealed lead-acid battery into the aircraft market [32]. ULM batteries have (i) thermally welded cells to ensure leak tightness, (ii) melanging of electrodes which ensures matched electrical performance characteristics for a batch of cells, (iii) seam welded plate tabs and copper cell links and terminals which provide lower resistance and minimise voltage drop, (iv) gas barrier membrane which prevents significant recombination and material migration, and (v) flooded gas barrier design that ensures the batteries to survive conditions which would destroy starved electrolyte sealed cells.

Fibre-structured nickel–cadmium (FNC) cells were first developed by Hoppeke in Germany. These cells are currently produced in large-scale by Acme Electric (USA) under a licence from Hoppeke. In FNC cells, two negative electrodes are arranged back-to-back with a highly porous recombination fibre-nickel structure in between two positive plates. The O$_2$ produced at the positive electrode during charge recombines rapidly at the recombination structure maintaining partial vacuum in the cell as shown in Fig. 18. Pressure does not build-up significantly even during C-rate overcharge. Low-pressure operation permits light weight plastic cell cases. The FNC cells utilise mechanically impregnated fibre electrodes for both negative and positive plates in addition to employing recombination plates in split negative design. The FNC cells offer significant improvement in energy density, life and cost over traditional sintered-plate cells.

Standard Ni–Cd cells, which have been the workhorse for storing electrical energy in spacecraft since the beginning of space exploration, use an aqueous chemical impregnation process for the fabrication of electrodes. During the preparation of electrodes by the chemical impregnation process
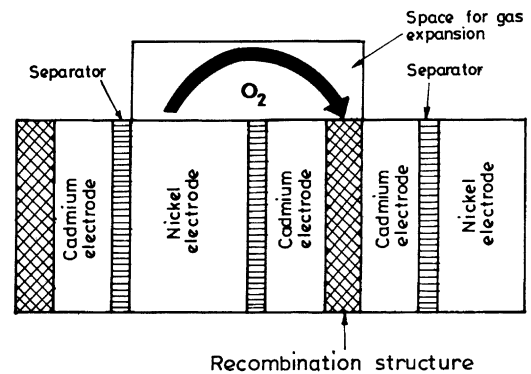
in acidic nickel/cadmium nitrate solution, a porous sintered nickel plaque is employed due to which the positive electrodes expand/swell considerably on cycling. Also, the non-woven nylon separator used in standard aerospace cells hydrolyses and contributes to cell failure. In order to improve the operational life of hermetically sealed Ni–Cd cells in spacecraft applications, super Ni–Cd cells were proposed by Hughes in the mid 1980s. In super Ni–Cd cells, the loading of positive and negative active materials into the porous sintered nickel structure is carried out electrochemically instead of by the vacuum impregnation process for conventional cells. Inert polymer impregnated zircar cloth, which is quite stable in the KOH electrolyte, replaces the polyamide separator. These changes have been found to be effective in extending the life of Ni–Cd cells both in low earth orbit (LEO) and geo-synchronous earth orbit (GEO) satellites. One of the main problems of these cells is the room temperature storage capacity loss in the discharged open or shorted conditions.

The aerospace division of Acme Electric (USA) has also introduced a sealed maintenance-free battery system based on the common vessel mono block (CVM) concept. The CVM concept can be adapted for virtually any type of battery utilising aqueous electrolyte. The CVM battery operates as a single sealed unit rather than individual sealed cells allowing the maximum performance without maintenance. The CVM battery comprises flooded cells and a metal-hydrogen regulator cell to consume H$_2$ and O$_2$ gases generated during charge, overcharge, discharge and storage. The cells share a common gas space with the regulator cell and there is constant gaseous flow among the cells regardless of whether H$_2$ or O$_2$ or both of these gases are consumed at the regulator cell kept at constant potential. Consequently, heat generation occurs only in the regulator cell. A smart charger monitors the battery pressure, current and the regulator cell current and temperature. The water balance among cells is maintained by means of water vapour transport in the common gas space. Since the heat generation during charge is limited to the regulator cell, it permits battery operation at high ($\sim$50°C) temperature with high charge-efficiency. The regulator cell current, temperature

and pressure are used to derive the SOC of the cells. The CVM battery is unique in offering no maintenance, fast-charge, excellent performance over a wide temperature range, high reliability and long cycle-life.

Ni–Cd cells suffer from a memory effect which is described as an apparent reduction in discharge voltage and capacity to a pre-determined cut-off voltage resulting from highly repetitive shallow charge–discharge cycle with very little overcharge. The memory effect is reflected as a step in the discharge curve of a cell. This is mainly observed in hermetically sealed aerospace Ni–Cd cells and does not occur normally during commercial use. But, in practice, the memory effect cannot exist (a) if the cells are charged to 100% of their actual capacity, (b) if the cells are discharged to variable depth in each cycle, and (c) if the cells are discharged below 1 V. Poor battery performance caused by simple correctable application problems often attributed to the memory effect are (a) high cut-off voltage, as cut-off voltage higher than 1.1 V per cell may drastically reduce the delivered capacity, and (b) high ambient temperature operation as high-temperature reduces charge acceptance at the normal $C/10$ rate. The discharge voltage is also lowered slightly. Hence, the capacity to a given cut-off voltage is lowered, creating the illusion of memory. Ni–Cd cells also have voltage depression due to continuous trickle charge. Voltage depression is principally a phenomenon associated with sintered electrodes. During extended period of over-charge, changes in morphology and composition of the sintered nickel oxide electrodes can create a resistance effect which typically depresses the discharge voltage up to about 100 mV per cell. Such a depression in cell voltage is more pronounced at high operating temperatures. The effect of long-term overcharge at elevated temperature on the dis-charge profile is shown in Fig. 19. The memory effect was initially attributed to the Cd electrode and, even today, the mechanism of this phenomenon is not fully understood. One of the explanations has been that the unused portion of the charged negative active material undergoes morphological changes causing additional voltage drop during discharge. Another opinion is that high-temperature overcharge favours the formation of intermetallic alloys, such as Ni_5Cd_{21}, which have a discharge potential more positive (ca. 150 mV) than the Cd electrode. The amount of intermetallic phases increases with the overcharge duration and the available capacity gradually decreases in the high-voltage plateau. Nickel hydroxide may be deliberately added or produced by corrosion of the sintered nickel substrate during the impregnation process. The solution to this problem is to eliminate or minimise nickel hydroxide in the Cd electrode. The alloy formation may be prevented by not using nickel as the substrate or current collector material in the negative electrode.

A freshly-charged positive electrode undergoes fairly fast self-discharge due to instability of the higher oxidation state of nickel (NiO_2) formed towards the end-of-charge. Charged positive active material is thermodynamically unstable and can spontaneously decompose with evolution of O_2 according to the reaction

$$2NiOOH + H_2O \rightarrow 2Ni(OH)_2 + \tfrac{1}{2}O_2 \qquad (18)$$
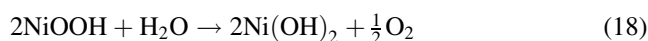
After termination of charge, gas evolution continues with the decomposition of the charged active material. The rates of decomposition and recombination depend on the temperature, structure of the active material and several other factors such as inter-electrode spacing, presence of gas diffusion membranes such as cellophane. The highly facile O_2 recombination reaction at the Cd electrode can accelerate the decomposition of positive active material according to reaction (17).

The positive and negative electrodes may contain nitrate ions which lead to nitrate (NO_3^-)–nitrite (NO_2^-) shuttle reactions due to the presence of impurities as described below.

$$NO_3^- + H_2O + 2e^- \rightarrow NO_2^- + 2OH^- \qquad (19)$$

$$NO_2^- + 5H_2O + 6e^- \rightarrow NH_3 + 7OH^- \qquad (20)$$

$$NO_3^- + H_2O + Cd \rightarrow NO_2^- + Cd(OH)_2 \qquad (21)$$

$$NO_2^- + 3Cd + 5H_2O \rightarrow NH_3 + 3Cd(OH)_2 + OH^- \qquad (22)$$

$$NH_3 + 7OH^- \rightarrow NO_2^- + 5H_2O + 6e^- \qquad (23)$$

$$NH_3 + 6NiOOH + H_2O + OH^- \rightarrow 6Ni(OH)_2 + NO_2^- \qquad (24)$$

$$NO_2^- + 2NiOOH + H_2O \rightarrow 2Ni(OH)_2 + NO_3^- \qquad (25)$$
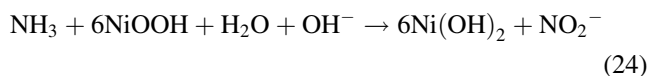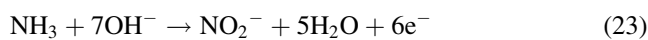
The NO_3^-–NO_2^- shuttle reaction continues until the cell is totally discharged or NH_3 is deactivated by the reaction

$$2NH_3 + 6NiOOH \rightarrow N_2 + 6Ni(OH)_2 \qquad (26)$$

leaving a permanent N_2 pressure within the cell. The capacity retention characteristics in Ni–Cd cells improve as the cell ages due to conversion of nitrate ions to N_2 gas.
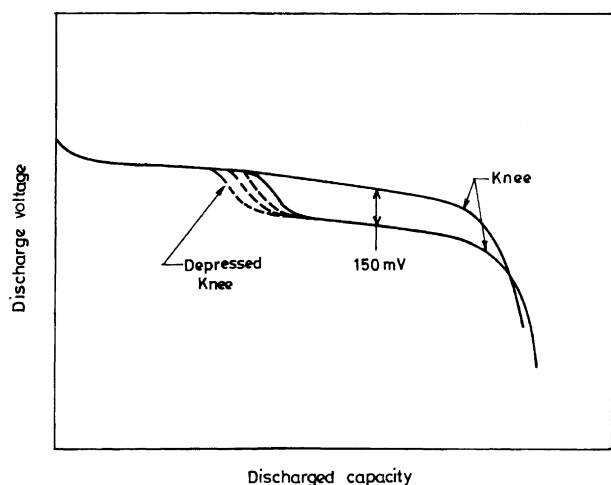

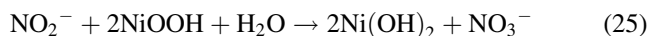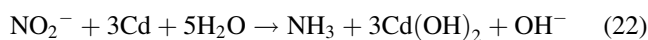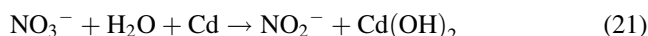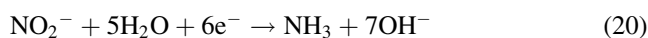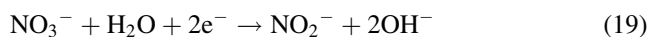Fig. 19. Effect of long-term overcharge on the discharge capacity of Ni–Cd cells at elevated temperatures.

Oxidation of organic impurities that are extracted or leached out from the separator at the positive electrode cause self-discharge of the cells. It is suggested that the main contributing factor is the decomposition of conventional polyamide separator with the production of ammonia and amines which participate in shuttle reactions similar to NO_3^- ions [33]. The charge retention can be drastically improved by using chemically stable separators such as polymer impregnated zircar or sulfonated polypropylene. It has been possible to decrease the self-discharge rate of Ni–Cd cells by incorporating certain inhibitors for the oxygen-evolution reaction, such as CdO, with the active material.

Ni–Cd cells exhibit higher than normal end-of-charge voltage on constant current charge after open-circuit-stand due to slow deactivation of the negative electrode. Permanent build-up of internal pressure may occur due to H_2 evolution if the charge voltage exceeds 1.5 V at room temperature (25°C). Besides, Ni–Cd batteries have a fairly high rate of self-discharge at high-temperatures. But worst of all, cadmium is an awful poison that can contaminate the environment. The unpopularity of cadmium has encouraged the development of alternate nickel-based batteries, namely Ni–H_2 and Ni–MH batteries.

4. Nickel–hydrogen batteries

In a Ni–H_2 cell, the cadmium electrode of the Ni–Cd cell is replaced with a light weight hydrogen-gas electrode which increases the gravimetric energy density of the cell significantly, but its volumetric energy density happens to be lower in relation to any other nickel-based battery. The system was specifically developed for aerospace applications. Initial development of Ni–H_2 cells was sponsored by COMSAT Laboratory, US Air Force and Hughes Aircraft Company for use in GEO and LEO satellites [34]. The COMSAT design uses an asbestos separator, a Teflon coating on the inner walls of the pressure vessel, and Zeigler seals for the feed-through terminals with the electrode leads running along the edges of the electrode stack. Hughes' design uses zirconium oxide separator, plasma sprayed zirconium oxide coating on the inner walls of the pressure vessel, Teflon compression feed-through terminals, and a 'pineapple slice' electrode configuration with electrode leads running through the centre of the stack allowing very short distances between the electrode stack and the pressure vessel wall [35]. There have been several modifications and improvements in Ni–H_2 batteries during the past several years [34]. The State-of-the-art, Ni–H_2 cell uses a combination of these two designs with ceramic or Zeigler feed-through terminals, single or two layers of zirconium oxide separator and plasma sprayed zirconium oxide coating on the inner walls of the pressure vessel [36]. Two types of electrode stacking configurations employed in the Ni–H_2 cells are (i) back-to-back stacking configuration shown in Fig. 20, and (ii) the recirculating design stacking in which the positive electrode, separator, negative electrode and gas screens are stacked sequentially.

Ni–H_2 cells have fewer inherent failure mechanisms than Ni–Cd cells and exhibit higher reliability and longer cycle-life. The other life-limiting component, namely the nylon separator, is replaced by zircar, a thin and porous zirconia ceramic sheet which reduces the electrolyte redistribution and improves the operational life of Ni–H_2 cells considerably in relation to Ni–Cd cells.

The charge–discharge reactions at the nickel electrode of a Ni–H_2 cell are the same as in Ni–Cd cell. The reaction at the hydrogen electrode during normal operation is
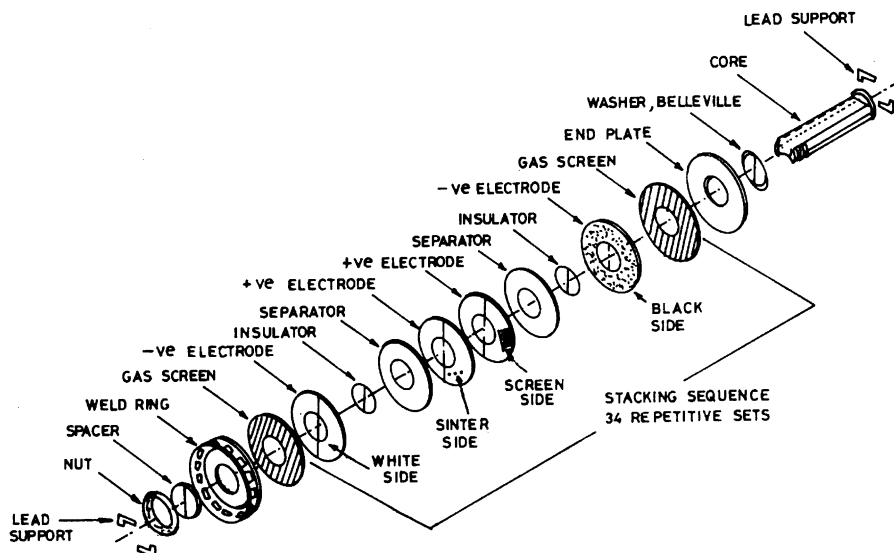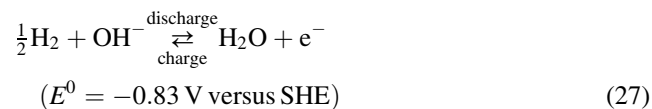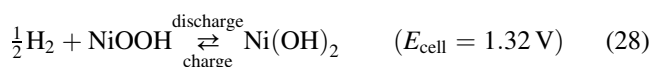
$$\frac{1}{2}H_2 + OH^- \underset{\text{charge}}{\overset{\text{discharge}}{\rightleftarrows}} H_2O + e^-$$

$$(E^0 = -0.83 \text{ V versus SHE}) \tag{27}$$

Fig. 20. Back-to-back stacking configuration in a Ni–H_2 cell.

Accordingly, the net cell reaction is

$$\tfrac{1}{2}H_2 + NiOOH \underset{charge}{\overset{discharge}{\rightleftarrows}} Ni(OH)_2 \qquad (E_{cell} = 1.32\,V) \qquad (28)$$

During overcharge O_2 is generated at the positive electrode which is electrochemically recombined at the catalytic platinum negative electrode. Since O_2 recombination at the negative platinum electrode is fast, the cell can sustain continuous overcharge at very high rates provided the heat generated is effectively dissipated to avoid any thermal run-away.

The parasitic reaction and reaction during overcharge at the nickel electrode is

$$4OH^- \rightarrow 2H_2O + O_2 + 4e^- \qquad (29)$$

The electrochemical reaction during overcharge of the hydrogen electrode is

$$2H_2O + O_2 + 4e^- \rightarrow 4OH^- \qquad (30)$$

The chemical recombination reaction at the negative electrode is

$$H_2 + \tfrac{1}{2}O_2 \rightarrow H_2O \qquad (31)$$

Depending on whether the capacity is limited by the nickel oxide electrode or the hydrogen electrode, one can have a positive-limited (hydrogen pre-charge) or negative-limited (nickel pre-charge) cell. All Ni–H_2 cells manufactured till the mid-1980s were H_2-pre-charge type. In a H_2-pre-charge cell, the reaction during reversal at the nickel electrode is

$$H_2O + e^- \rightarrow OH^- + \tfrac{1}{2}H_2 \qquad (32)$$

In a H_2-pre-charge cell, during reversal the normal discharge reaction taking place at the H_2 electrode is

$$\tfrac{1}{2}H_2 + OH^- \rightarrow H_2O + e^- \qquad (33)$$

During reversal of a nickel pre-charged cell, the normal discharge reaction proceeding at the nickel electrode is

$$2NiOOH + 2H_2O + 2e^- \rightarrow 2Ni(OH)_2 + 2OH^- \qquad (34)$$
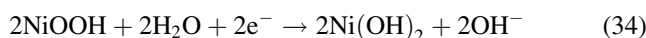
In a nickel pre-charged cell, O_2 evolution occurring at the H_2 electrode during reversal is

$$4OH^- \rightarrow 2H_2O + O_2 + 4e^- \qquad (35)$$

The net reaction during reversal of a positive pre-charged cell is given as

$$2NiOOH + H_2O \rightarrow 2Ni(OH)_2 + \tfrac{1}{2}O_2 \qquad (36)$$
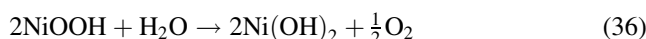
When a positive pre-charge cell is forced into reversal after all the H_2 is consumed, O_2 is generated at the H_2 electrode until the positive nickel oxide electrode is fully-discharged. The generated O_2 is consumed during recharge of the cell. During reversal of a nickel positive pre-charge cell, there is a possibility for formation of an explosive mixture of H_2 and O_2 in the cell.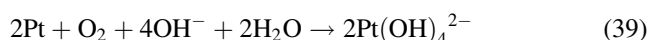 The O_2 evolution reaction at the platinum electrode can also cause dissolution of platinum at the negative electrode according to the reaction
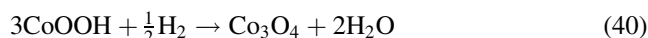
$$2Pt + O_2 + 4OH^- + 2H_2O \rightarrow 2Pt(OH)_4^{2-} \qquad (37)$$
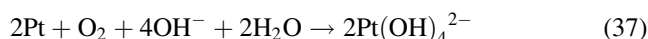
Reactions at the hydrogen electrode during shorted storage of cells with nickel pre-charge are

$$4OH^- \rightarrow 2H_2O + O_2 + 4e^- \qquad (38)$$

and

$$2Pt + O_2 + 4OH^- + 2H_2O \rightarrow 2Pt(OH)_4^{2-} \qquad (39)$$

The electrode reaction during storage in cells with hydrogen pre-charge is

$$3CoOOH + \tfrac{1}{2}H_2 \rightarrow Co_3O_4 + 2H_2O \qquad (40)$$

Since cobalt is an essential component of these electrodes this results in permanent capacity loss of the Ni–H_2 cells.

Ni–H_2 cells are mainly employed in spacecraft for on-board energy conversion and storage. Various configurations of Ni–H_2 spacecraft batteries are (a) independent pressure vessel (IPV) batteries, (b) common pressure vessel (CPV) batteries, (c) single pressure vessel (SPV) batteries, (d) dependent pressure vessel (DPV) batteries, and (e) bipolar batteries.

IPV batteries contain only one cell stack per pressure vessel. In common pressure vessel batteries, there are two or more cell stacks electrically connected in series. A two cell CPV design provides 50% reduction in cell mounting foot print with the number of cell units less than the IPV design. There is a 30% reduction in battery volume and 15% reduction in battery mass. In SPV design, the required number of cells forming the battery are electrically connected in series and placed in a single pressure vessel. This design offers advantages of reduction in mass, volume and cost. The major disadvantage is that failure of any one cell results in failure of the entire battery. The SPV batteries can be configured to deliver a wide range of capacities and voltage outputs. The SPV batteries are less reliable than IPV and CPV cells. The DPV technology is a modular approach to Ni–H_2 space battery design [37].

The basic Ni–H_2 cells comprise a stack of electrodes with alternating pairs of positive nickel and negative hydrogen electrodes separated from each other with a zircar separator wetted with potassium hydroxide electrolyte solution so as to provide electronic insulation and ionic conduction between the anode and the cathode, and all contained in a cylindrical pressure vessel with hemispherical end caps provided with hermetically sealed feed-through terminals for the electrodes. The pressure vessel of a Ni–H_2 cell is highly prone to single point failure. Therefore, identification of fracture critical flaws on the surface of the material or at a welded seam is important. The vessel must meet the criteria established in MIL-STD 1522A for hermeticity and strength. The pressure vessel design should have a burst strength three times the maximum expected operating

pressure. The terminal bosses are injection moulded with Nylon bushing which, when crimp fitted to the cell terminal, form the Ziegler compression seal to provide hermeticity. Its exceptional strength precludes terminal rotation during normal handling, testing and battery assembly.

The cell stack in back-to-back configuration is assembled on a moulded plastic (polysulfone) core which is channelled to accommodate plate lead bundles. The polysulfone core provides light weight, high strength and compatibility with caustic electrolyte. The stack is confined between two polysulfone end plate assemblies. Belleville spring washers permit uniform stack compression and help accommodating positive-plate growth.

The negative hydrogen electrode consists of a Teflon-bonded platinum black catalyst supported on a fine mesh nickel screen with a microporous gas-diffusion Teflon backing film. The catalyst loading is about 5–8 mg cm^{-2}. The microporous Teflon backing membrane avoids water/electrolyte loss from the rear of the negative platinum electrode during charge and overcharge while readily allowing diffusion of hydrogen and oxygen gases. A photo-etched nickel substrate eliminates cut edges of the electrodes that could cause shorting during cell stack assembly and provides solid tabs for lead attachment. Hydrogen electrode should provide the right interface for the electrochemical reactions to occur without flooding or drying out the electrodes at the separator interface.

The positive plate consists of 35 mil ($\sim$1 mm) thick dry sintered porous nickel plaques electrochemically impregnated with nickel hydroxide active material to the extent of 1.65 g cm^{-3} of void volume. A pure nickel wire mesh substrate is centred in the electrode structure to provide electrical and structural benefits. A bend strength of 900 psi is ensured for the sintered nickel plaque at 84% porosity level to provide long-term dimensional stability to the electrodes. The plate typically delivers a capacity greater than 125% of the theoretical value (calculated for one electron transfer reaction) during flooded capacity checks at the component level.

In older designs, non-woven asbestos was used as the separator material which offers high bubble pressure and prevents rapid recombination of H$_2$ and O$_2$ at the negative electrode. A pressure differential of more than 25 psi is required to force O$_2$ bubbles through the separator. Asbestos has dual pore size distribution which helps preventing separator dryout. Currently, ZYK-15H untreated knit cloth type zircar separator is exclusively used in all hermetically sealed aerospace Ni–H$_2$ cells. Zircar has very good stability in the caustic electrolyte allowing long-term storage and/or cycling. Cells with zircar separator have lower impedance and better discharge voltage performance. Zircar has low bubble pressure and allows permeation of O$_2$ gas for recombination at the negative electrode. Zircar tends to retain the thickness under compression and holds relatively more electrolyte per unit volume of the separator. But, it is very fragile and must be handled with care.

A polypropylene gas spacer screen is used within the stack for gas management.

At present, state-of-the-art Ni–H$_2$ cells use nickel pre-charge where the capacity of the cell is limited by the negative active material on discharge. Some of the design parameters such as bend strength of the positive sinter, loading level of the positive electrode and the concentration of the electrolyte strongly influence the cycle-life of Ni–H$_2$ cells. Higher concentration of electrolyte stabilises higher oxides of nickel and the electrode capacity increases with electrolyte concentration between 21 and 38% aqueous KOH in Ni–H$_2$ cells. There is ample evidence that lower concentration of electrolyte reduces corrosion of the sintered-nickel substrate, as also the plate growth especially in high-porosity sintered-plates, but at the cost of lower capacity. Generally, lower concentration of electrolyte (26% aqueous KOH) is recommended for LEO satellites while a higher concentration of electrolyte (31% aqueous KOH) is used in GEO satellites. Cells without nickel pre-charge are often found to develop low capacity and/or a second plateau below 1 V level after a prolonged storage period. Nickel pre-charge has been tested by numerous independent investigators in the industry with pronounced beneficial effects. The principal benefit is the reduction of capacity decay on storage. In addition, nickel pre-charge provides better charge-retention, lower charge-voltage, a slightly higher discharge voltage and lower operating pressure for the cell. Accordingly, the cell weight is reduced.

A catalysed wall wick serves as electrolyte concentrator and inventory equilibrator and as a reservoir. The vessel wall is coated with yttria-stabilised zirconia by a plasma spraying technique to form a porous layer to serve as wall wick. Since the H$_2$–O$_2$ recombination reaction is highly exothermic, it is desirable to locate the recombination sites close to the heat removal mechanism. This is done by coating the wall wick with platinum black to form strips of catalytic sites where the H$_2$–O$_2$ recombination reaction can occur. In cells, where a passive cooling system is used, heat is removed from the pressure vessel wall. The advantage of producing H$_2$–O$_2$ recombination outside the stack and on the wall of the pressure vessel is the ease of heat rejection. The catalysed wall wick also allows the cell to run cooler.

Foam electrodes which were introduced in the mid 1980s function akin to sintered-plate electrodes. A nickel frame work with approximately 95% free volume is created by nickel plating a porous synthetic material comprising polyurethane or acrylic fibre and subsequent pyrolysis of the plastic material. The utilisation of active material in these electrodes was poorer than in sintered-plates. The higher pore volume and larger active material holding capacity (reduction in conducting substrate weight) more than compensates for the loss of utilisation efficiency and consequently improves the energy density of the cell.

Independent pressure vessel (IPV) Ni–H$_2$ batteries suffer from inefficient grouping of multiple cylindrical cells in the battery pack. DPV design offers a higher energy density and

reduced cost with an efficient mechanical, electrical and thermal cell configuration in addition to a reduced parts count. A unique feature of the DPV cell design is the prismatic electrode stack which provides an optimum geometry for the pressure vessel. The flat sides of the pressure vessel are supported by the end plates in the final battery assembly. Dependent pressure vessel geometry requires the cell to be externally supported to contain the hydrogen pressure developed inside the cell during charging. Since the pressure vessel is not required to sustain the full internal pressure, it is made thinner to reduce the weight. The round edge of the pressure vessel over a relatively small radius efficiently supports the full internal pressure with minimum weight of the pressure vessel material. The pressure vessel is made of stainless steel and consists of two identical seamless halves with a lip around the edge where the two halves meet to assist in laser welding for hermetically sealing the cell. One of the pressure vessel halves is fitted with cell terminal bosses and a fill tube. The cell terminal uses an internal boss arrangement which has minimum external protrusion and minimises overall dimensions of the cell.

The electrode stack consists of nickel oxide and hydrogen electrodes interspersed with absorbent polymeric separator material. A back-to-back arrangement with each nickel electrode facing the catalyst side of the hydrogen electrode is employed. In this arrangement, the hydrophobic sides of the hydrogen electrodes face each other. A gas spacer is inserted in order to facilitate gas diffusion towards and away from the hydrogen electrode during charge and discharge reactions.

A metal stacking bracket spot welded to one half of the pressure vessel holds the electrode stack in place within the cell pressure vessel. The stack is kept electrically isolated from the stacking bracket and the pressure vessel. The electrical tabs emerge through a window in the stacking bracket. The positive and negative lead bundles from the stack are given stress relief loops before attachment to terminal posts to prevent any mechanical stress owing to launch vibrations being transmitted to the electrode/tab connection. The cells are connected in series to form the battery assembly. In a DPV battery assembly, the cells are sandwiched between two end plates which is a standard practice in Ni–Cd battery assembly for satellite applications. Battery-to-cell weight ratio is an important figure-of-merit for spacecraft applications. The battery-to-cell weight ratio is significantly lower for DPV batteries in comparison to standard IPV batteries. Generally, cells are arranged in two arrays to form the battery assembly to provide a compact and nearly square package for ease of integration into the spacecraft. To accommodate an odd number of cells, generally a dummy cell is used which adds to the battery mass, but does not contribute to energy storage.

The electrical design includes aspects and components such as intercell connection, conductor losses, the battery electrical interface, battery voltage, current and temperature monitoring, charge controllers, and battery electronics,

namely strain gauges, strain gauge amplifiers, heaters, heater controllers, cell by-pass modules, cell voltage, current and temperature monitoring depending on the specific battery design. Strain gauge circuitry, in a full bridge configuration, measures the microflex of the pressure vessel produced by the internal pressure changes in the cell. The strain gauge is calibrated after girth weld closure before electrolyte activation by pressurising the cell with helium. The strain gauge bridge has to be excited with a dc supply (2–10 V) and the output has to be amplified and processed to directly indicate the cell internal pressure and the cell SOC. Three thermistors mounted at different locations in the battery are used to check the uniformity of temperature across the battery. A non-contact inductive type current sensor is used to sense the battery current. All monitoring information such as voltage, current, temperature and pressure are sent to telemetry through a battery electrical interface connector.

In order to achieve a long life, the Ni–H$_2$ battery has to be operated within a narrow band of temperature. Cell heaters are used to help regulate cell temperature during orbital operation. The cell reaction is endothermic during the bulk of charging, and exothermic during overcharge and discharge. The heat generated in the cell has to be conducted to the spacecraft deck and subsequently radiated to space. In DPV batteries, a thin aluminium thermal shim, which is electrically insulating and thermally conducting, is inserted between each pair of adjacent cells such that the flat side of the pressure vessel makes contact with each cell through a thermal shim. Each thermal shim has a flange which contacts the battery base plate and acts as a heat sink. This arrangement provides a large cross-sectional area for removal of heat from the internal electrode stack. In DPV batteries, the electrode stack is in direct contact with the flat pressure vessel wall. By contrast, in IPV cells, the stack is not in direct contact with the cylindrical pressure vessel and heat can only be rejected by the electrode stack across a narrow hydrogen gap between the stack and the pressure vessel wall. DPV batteries provide a direct path for heat rejection by the cell. DPV batteries use advanced fibre-based nickel electrodes which have ca. 25% higher specific energy than standard sintered-nickel aerospace electrodes. But, the fibre-based nickel electrodes are to be qualified for space applications. Testing and qualification of the fibre nickel electrodes are important issues which are currently being addressed. DPV cells provide energy density of 60 Wh kg^{-1} and 73 Wh l^{-1} in comparison to an IPV cell which provides only 53 Wh kg^{-1} and 52 Wh l^{-1}. The high energy version of DPV cells which use fibre nickel electrodes can provide 76 Wh kg^{-1} and 89 Wh l^{-1}. The advanced design DPV cells can provide up to 70 Wh kg^{-1} at full battery level as against 42 Wh kg^{-1} provided by the state-of-the-art IPV batteries [36]. Developing a light weight pressure vessel capable of containing hydrogen at around 1000 psi requires innovative design, careful materials selection and manufacturing techniques. A hydroforming process is considered to be most

suitable for this application. Ni–H$_2$ batteries have certain deficiencies such as low volumetric energy density, high self-discharge rate, capacity loss on storage, high thermal dissipation during high rate discharge, and safety hazards due to high operating pressures. The low volumetric energy density of the Ni–H$_2$ batteries is overcome in the Ni–MH battery system.

5. Nickel–metal hydride batteries

There is continuous effort to develop high energy density, high power density and low-cost rechargeable batteries to meet the ever increasing needs for spacecrafts, defence, communication, electric vehicles, computers, camcorders, cellular phones, power tools and other home appliances. Until recently, mainly Ni–Cd batteries were meeting these requirements. Ni–MH batteries using hydrogen storage alloys as the negative electrode material have been drawing increasing attention due to their higher energy density both in terms of weight and volume, improved high rate capability (the endothermic nature of the discharge reaction allows high rate discharge with relatively less heat dissipation), and high tolerance to overdischarge. Furthermore, sealed Ni–MH cells can be easily constructed because the O$_2$ and H$_2$ gas evolved, respectively, during overcharge and overdischarge are effectively consumed allowing prismatic design with superior packaging and heat management capabilities. These batteries are also free from dendrite formation and memory effect due to recrystallisation and are devoid of toxic materials such as lead, cadmium, mercury and asbestos although nickel is known to present health hazards to humans.

Akin to the Ni–Cd system, Ni–MH cells also employ nickel positive plates with NiOOH as the active material and an aqueous KOH electrolyte. The main difference is that the active material in the negative plate is hydrogen absorbed in a metal alloy. The metal alloys in which hydrogen is stored fall into two categories: (a) the AB$_5$-alloys based on mixtures of nickel and rare earth, and (b) the AB$_2$-alloys based on nickel commonly blended with titanium, vanadium and zirconium. A typical composition of the AB$_5$-alloy that has been documented to be a promising electrode material is Mm (Mm = misch-metal: 25 wt.% La, 50 wt.% Ce, 7 wt.% Pr, 18 wt.% Nd) Ni$_{3.2}$Co$_{1.0}$Mn$_{0.6}$Al$_{0.11}$Mo$_{0.09}$ which has CaCu$_5$-type crystal structure. Among the AB$_2$-type alloys, Ti$_{0.51}$Zr$_{0.49}$V$_{0.70}$Ni$_{1.18}$Cr$_{0.12}$ has been found to be an attractive electrode material which has ^{14}C-Laves crystal structure. In the beginning, AB$_5$-type alloys were employed as battery electrodes, but at present, AB$_2$-type alloys are preferred electrode materials for Ni–MH batteries [38]. It is found that while AB$_2$-type alloys yield superior energy storage densities, the AB$_5$-alloys are able to hold hydrogen better, thus, lowering the self-discharge rate of the battery. Besides, AB$_5$-alloys happen to be less expensive and easier to use.

Historically, hydrides of binary intermetallic compounds were first reported by Trzesciak et al. in 1956 [39]. In 1958, Libowitz demonstrated reversible hydrogen absorption and desorption in ZrNiH$_3$ [39]. Soon other intermetallic hydrides such as LaNi$_5$ (AB$_5$-alloy) which could absorb and desorb large amounts of hydrogen were discovered [39]. Justi et al. [40] were the first to investigate NiTi hydrides as reversible hydrogen electrodes. During 1970s and 1980s, Daimler Benz [41] carried out extensive studies on NiTi$_2$ (AB$_2$-alloy) and NiTi (AB-alloy) intermetallic materials as hydrogen storage materials for vehicular applications. Early studies on Ni$_2$Ti-based AB$_2$ and AB alloys and LaNi$_5$-based AB$_5$-alloys were found to have cycle lives which were too poor to be useful for practical batteries [42]. Guegan et al. [43] were first to recognise the correlation between the gaseous pressure-composition isotherm and the electrochemical properties of LaNi$_5$-based alloys. Willems [44] suggested that the long-term stability of LaNi$_5$ electrodes can be improved dramatically by partly replacing La and Ni by other alloying elements, especially Co which is both expensive and toxic. It was realised that partial substitution of Cr and/or Ge for Ni in LaNi$_5$-type alloys also improves the performance of MH electrodes.

Most of the early studies on metal hydride alloys were based on binary alloys which had the limitation of stability, poor hydrogen storage capacity and life. Fig. 21 shows the types of metal hydride formed between hydrogen and various other elements in the periodic table. The diverse properties required for a superior MH battery electrodes are appropriate hydrogen binding energy, high hydrogen absorption/storage capacity, fast electrode kinetics, good H$_2$–O$_2$ recombination rate, charge retention, chemical and physical stability (oxidation/corrosion resistance), easy manufacturability at a reasonable cost which can be achieved through compositional and structural disorder in multicomponent, mutiphase alloys introduced by specific elemental modifiers [45,46]. According to Ovishinsky, a typical disordered material contains five distinct compositional phases and body-centred cubic, hexagonal and ^{14}C-Laves crystal structures. Body-centred cubic structures can store large quantities of H$_2$, but lack electrocatalytic activity. The hexagonal and ^{14}C-Laves phases effectively channel H$_2$ for rapid electrochemical discharge. The basic multielement multiphase alloys typically contain V, Ti, Zr, Ni, Cr, Co, Mn and Fe. The alloying constituents, Ti, Zr and V primarily provide H$_2$ absoption, Co and Mn provide surface activity, Ni provides catalytic activity for redox reaction and Cr and Fe provide corrosion resistance [47,48].

At present, most commercial Ni–MH batteries either employ AB$_5$-type MmNi$_{3.2}$Co$_{1.0}$Mn$_{0.6}$Al$_{0.11}$Mo$_{0.09}$ or AB$_2$-type Ti$_{0.51}$Zr$_{0.49}$V$_{0.70}$Ni$_{1.18}$Cr$_{0.12}$ alloys. The commonly used misch-metal alloys are capable of delivering a capacity of only about 300 Ah kg^{-1}. While these alloys utilise Ovishinsky's concept of disorder, they do not compare to commercial Ovonic transition metal alloys which exhibit a capacity of ~400 Ah kg^{-1} and provide 80 Wh kg^{-1} of

* FORMS IONIC HYDRIDE
● FORMS COVALENT HYDRIDE
Δ FORMS METALLIC HYDRIDE
□ REQUIRES >1 ATM H_2 TO FORM HYDRIDE
⊛ THESE HYDRIDES CANNOT BE PREPARED BY DIRECT REACTION
(+) FORMATION OF HYDRIDE IS ENDOTHERMIC
(−) FORMATION OF HYDRIDE IS EXOTHERMIC

Fig. 21. Periodic table showing types of metal-hydrides.

specific energy at cell level. This jump is only considered as a first threshold to the projected capacity value of 700–1000 Ah kg^{-1} in future phases. Mg-based alloys have been projected as excellent materials for MH electrodes with capacity values as high as 1000 Ah kg^{-1} [49]. But, magnesium based alloys are prone to corrosion in alkaline environments. The major problems associated with these alloys are the sluggish hydriding kinetics at room temperature and

oxidation of the material under ambient environmental conditions [50].

Fig. 22 gives the operating principle of a sealed rechargeable Ni–MH cell. The Ni(OH)$_2$ at the positive electrode is oxidised to NiOOH on charge and reduced back to Ni(OH)$_2$ during discharge. During charge, at the MH negative electrode, reduction of water produces atomic, adsorbed hydrogen which diffuses into the lattice of the intermetallic alloy

REACTIONS AT THE NEGATIVE ELECTRODE

$$M + H_2O + e^- \longrightarrow MH + OH^-$$
$$1/2\,O_2 + 2MH \longrightarrow 2M + H_2O$$
$$O_2 + 2H_2O + 4e^- \longrightarrow 4OH^-$$

$$MH + OH^- \rightleftarrows M + H_2O + e^-$$

$$H_2 + 2OH^- \longrightarrow 2H_2O + 2e^-$$

REACTIONS AT THE POSITIVE ELECTRODE

$$4OH^- \longrightarrow 2H_2O + O_2 + 4e^-$$

$$NiOOH + H^+ + e^- \rightleftarrows Ni(OH)_2$$
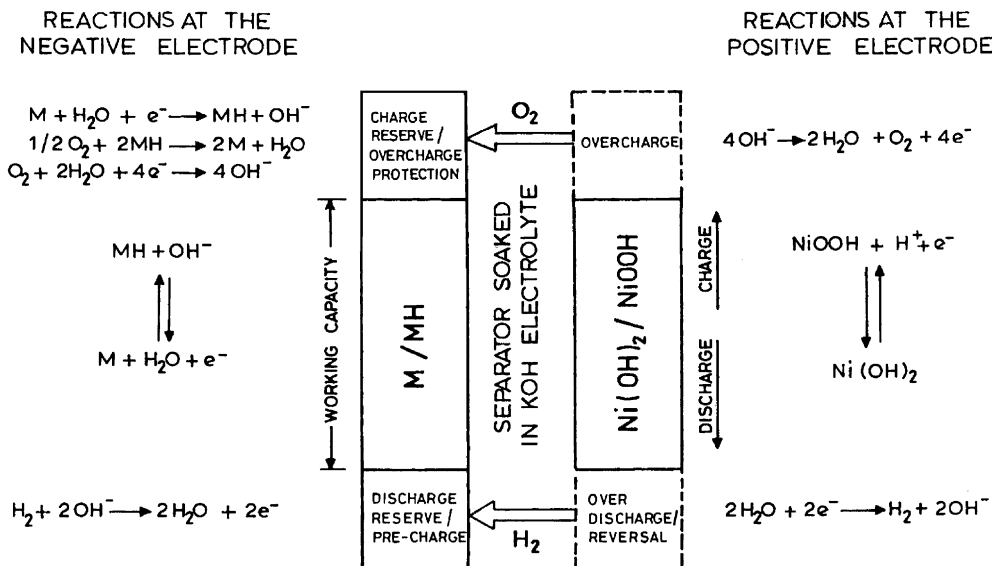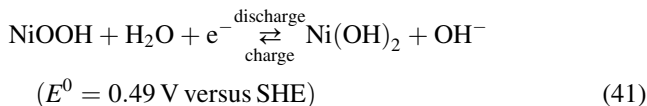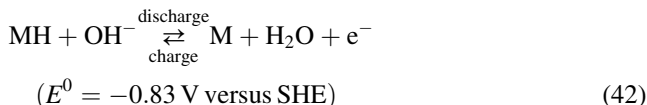
$$2H_2O + 2e^- \longrightarrow H_2 + 2OH^-$$

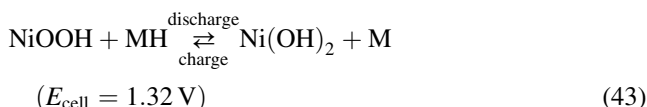Fig. 22. Design principle of a sealed Ni–MH cell.

to form a metal hydride. A reverse reaction takes place during discharge. Accordingly, the electrochemical reactions occurring in a Ni–MH cell can be represented as follows:

$$NiOOH + H_2O + e^- \underset{\text{charge}}{\overset{\text{discharge}}{\rightleftarrows}} Ni(OH)_2 + OH^-$$

$$(E^0 = 0.49 \text{ V versus SHE}) \tag{41}$$

and

$$MH + OH^- \underset{\text{charge}}{\overset{\text{discharge}}{\rightleftarrows}} M + H_2O + e^-$$

$$(E^0 = -0.83 \text{ V versus SHE}) \tag{42}$$

Accordingly, the overall cell reaction is

$$NiOOH + MH \underset{\text{charge}}{\overset{\text{discharge}}{\rightleftarrows}} Ni(OH)_2 + M$$

$$(E_{\text{cell}} = 1.32 \text{ V}) \tag{43}$$

The charge–discharge reactions in a Ni–MH battery proceed via a homogeneous solid-state mechanism through proton transfer between nickel hydroxide and hydrogen storage alloy distinguishing it from other nickel-based batteries where the anode reaction proceeds through a dissolution–precipitation mechanism. Hence, the source of many of the performance deficiencies, such as (a) changes in crystallography, (b) changes in mechanical integrity, (c) changes in surface morphology of the electrode as a result of dissolution and recrystallisation, and (d) reduced electrical conductivity in the oxidised state, are eliminated in the Ni–MH system permitting a more compact assembly, longer cycle-life and the construction of a solid-state battery using a proton conducting solid electrolyte [51,52].

As in the Ni–Cd cell, the electrolyte is concentrated aqueous KOH. As a consequence of reactions (41) and (42), there is no net change in the electrolyte quantity or concentration over the charge–discharge cycles. This is an attractive feature of Ni–MH batteries over Ni–Cd batteries wherein water is generated during charge and consumed during discharge. On the down side, Ni–MH batteries deliver less power, have a faster self-discharge and are less tolerant to overcharge like the Ni–Cd batteries.

Since the nickel oxide electrode is thermodynamically unstable in the cell environment, oxygen-evolution occurs at this electrode as a parallel and competing reaction. The parasitic reactions during charge are represented by

$$4OH^- \rightarrow 2H_2O + O_2 + 4e^- \tag{44}$$

and

$$H_{\text{adsorbed}} + H_{\text{adsorbed}} \rightarrow H_2 \tag{45}$$

To ensure proper functioning of a sealed Ni–MH cell under a variety of conditions, it is designed in such a way that the capacity of the cell is limited by the positive electrode. Accordingly, O_2 evolution occurs at the positive electrode during overcharge and this diffuses to the metal-hydride

electrode where it combines to form water. The negative to positive capacity ratio varies between 1.5 and 2. Typically, the discharge reserve is in the range of 20% of the positive capacity.

Reactions during cell overcharge are

$$4OH^- \rightarrow 2H_2O + O_2 + 4e^- \tag{46}$$

$$M + H_2O + e^- \rightarrow MH + OH^- \tag{47}$$

$$4MH + O_2 \rightarrow 4M + 2H_2O \tag{48}$$

Under deep-discharge conditions, due to the inevitable difference in storage capacities of series connected cells in a Ni–MH battery, H_2 evolution occurs at the positive electrode which is oxidised to water at the MH electrode. Thus, there are recombination mechanisms for both H_2 and O_2 gases evolved during overdischarge and overcharge, respectively, permitting sealed operation of the Ni–MH cells. Reactions during cell overdischarge are

$$H_2O + e^- \rightarrow \tfrac{1}{2}H_2 + OH^- \tag{49}$$

and

$$H_2 + 2OH^- \rightarrow 2H_2O + 2e^- \tag{50}$$

Since the cell reaction causes no net change in the electrolyte concentration or quantity, maintenance of electrolyte concentration results in good gas recombination, good high and low temperature operations, and good resistance to cycle-life limitations caused by corrosion and swelling.

Ni–MH cells are generally available in 'AA', 'sub-C' and 'C' sizes. Prismatic cells up to 250 Ah are manufactured for electric vehicle application by Ovonic Battery Company (USA) and Gold Peak Industries (Hong Kong). The capacity that can be obtained from a Ni–MH cell is about two times of an equivalently sized Ni–Cd cell. The Ni–MH cells can operate from -20 to $+45°C$. But, above $+45°C$, the charge efficiency falls steeply. The charge efficiency of Ni–MH cell is better than Ni–Cd cells for charge rates between $C/10$ and $C/20$ at $20°C$. The voltage and temperature profiles during charge at various rates are given in Fig. 23. The typical voltage profile during charge at different temperatures is given in Fig. 24. The internal pressure of the cell generally does not exceed 50 psi for a $C/10$ charge at $20°C$. Typical profile of internal pressure during charge at various rates is shown in Fig. 25. The cell pressure increases both at higher charge rates and at higher temperatures. Cylindrical cells are provided with a safety vent operating at around 400 psi. Due to the endothermic nature of the discharge process, the heat evolved during discharge is relatively less than in Ni–Cd cells at discharge rates less than C. Joule heating masks the cooling due to endothermic desorption of H_2 during discharge. Cells can be discharged even at the $5C$ rate. The dependence of the discharge rate and the discharge capacity is depicted in Fig. 26. The effect of temperature on available capacity is given in Fig. 27. The absorption of H_2 during charge is an exothermic process. But the temperature rise becomes noticeable only from the point
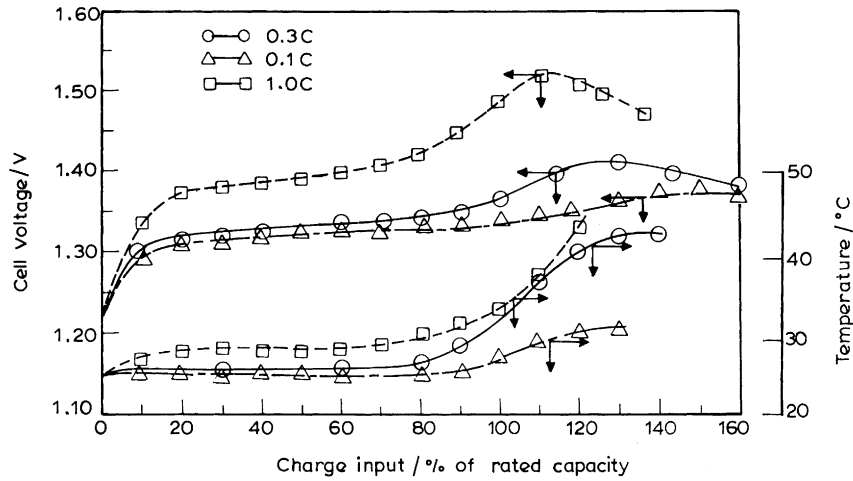
Fig. 23. Typical voltage and temperature profiles for a Ni–MH cell during charge at various rates.
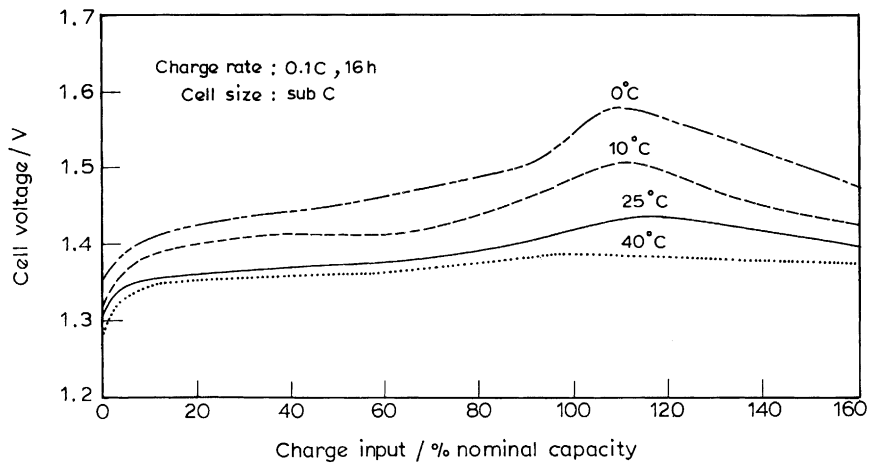

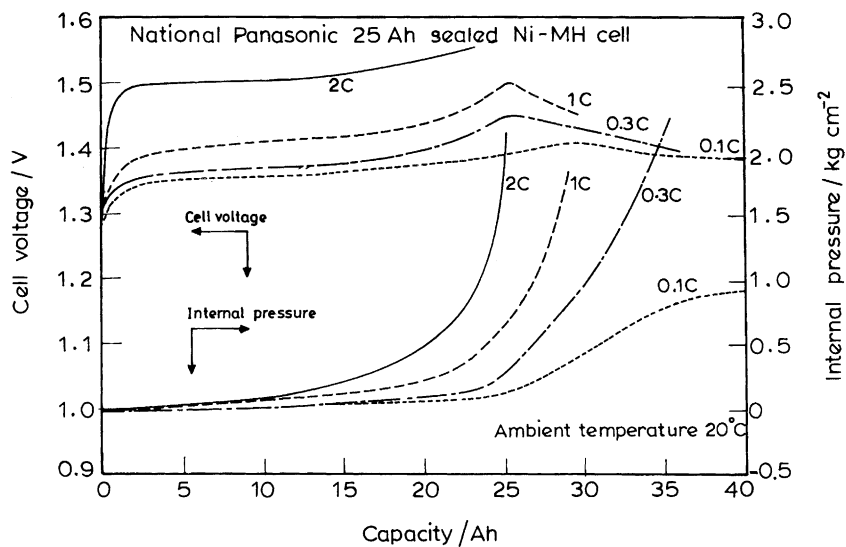Fig. 24. Voltage profile for a Ni–MH cell during charge at different temperatures.

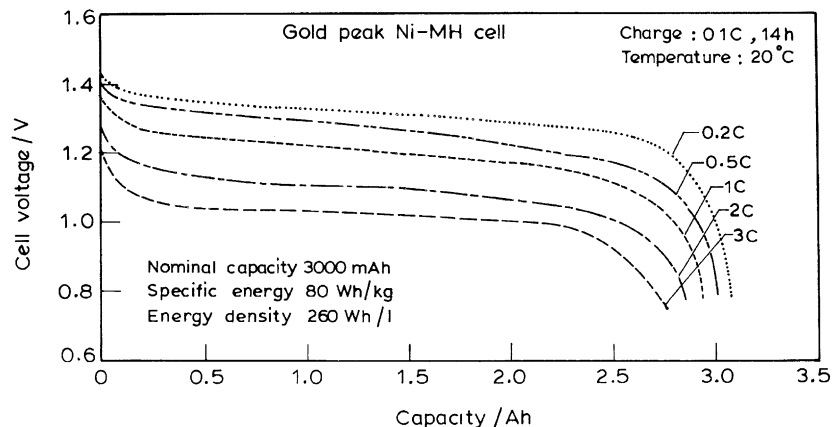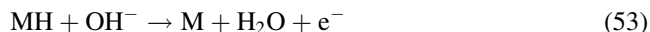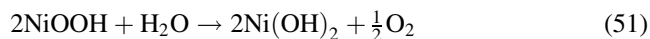Fig. 25. Pressure profile for a Ni–MH cell during charge at various rates.

Fig. 26. Effect of discharge rate on capacity of a Ni–MH cell.

where O_2 recombination begins to occur. During hydriding, the electronic conductivity decreases. If the overcharge is controlled then the heat generation in the cells is mainly due to Joule heating. Cells can be charged at C rate. Monitoring the inflection of charge voltage is considered to be the most appropriate method to prevent overcharge, and thus, to improve the cycle-life of the cell. A cycle-life >1000 cycles at 100% depth-of-discharge (DOD) has been demonstrated. Cycling at $C/3$ (charge for 65 min and $C/1.6$ discharge for 35 min) at 40% DOD with an overcharge factor of 1.02 at 22°C has been carried out for over 8000 cycles. Under similar conditions, a Ni–H_2 cell requires 1.1 overcharge factor. Ni–MH cells have a higher rate of self-discharge in relation to Ni–Cd cells.

Charged positive active material is thermodynamically unstable and can spontaneously decompose with evolution

of O_2 according to following reactions:

$$2NiOOH + H_2O \rightarrow 2Ni(OH)_2 + \tfrac{1}{2}O_2 \tag{51}$$

$$O_2 + 2H_2O + 4e^- \rightarrow 4OH^- \tag{52}$$

$$MH + OH^- \rightarrow M + H_2O + e^- \tag{53}$$

$$4MH + O_2 \rightarrow 4M + 2H_2O \tag{54}$$

The highly facile O_2 recombination reaction at the MH alloy electrode can accelerate the decomposition of the positive active material. Gaseous hydrogen, which is in equilibrium with the metal hydride alloy, can reduce the charged positive electrode as indicated below.

$$2NiOOH + H_2 \rightarrow 2Ni(OH)_2 \tag{55}$$
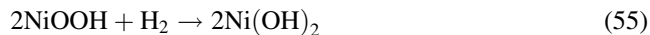
It is noteworthy that H_2 oxidation is inhibited by anodically formed $Ni(OH)_2/NiOOH$. But cathodically deposited

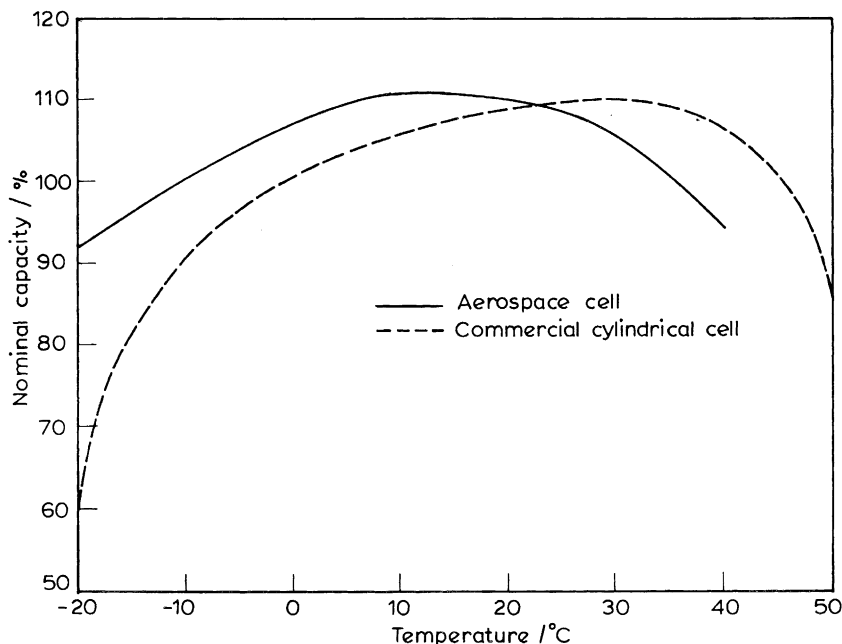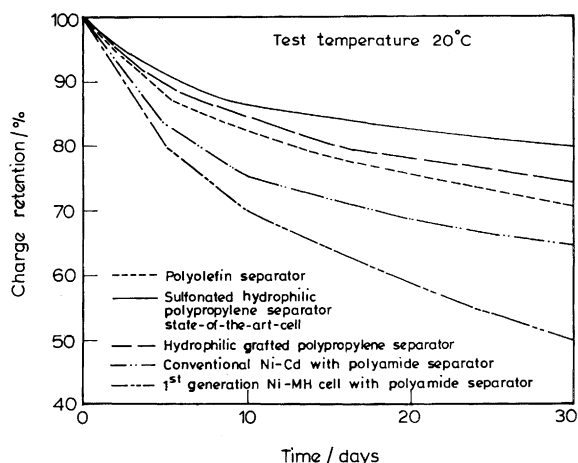Fig. 27. Effect of temperature on available capacity of Ni–MH cells.

Fig. 28. Comparison of charge-retention characteristics of Ni–MH cells.

Ni(OH)$_2$ does not inhibit the reaction to the same degree. Shuttle reactions due to the presence of impurities, such as nitrate present in the electrodes and the electrolyte, contribute to self-discharge to a significant extent in a fresh cell. Oxidation of organic impurities that are extracted or leached out from the separator at the positive electrode also contribute to the self-discharge process. Metal ions leached out from the MH alloy may have an adverse reaction at the positive electrode. It is reported [33] that the main contributing factor to the decomposition of the conventional polyamide separator is the production of ammonia and amines which participate in shuttle reactions similar to NO$_3^-$ ions in Ni–Cd battery. Charge retention can be drastically improved by using chemically stable separators such as sulfonated polypropylene. Fig. 28 depicts the comparison of charge retention characteristics of Ni–MH cells with different separator materials. Addition of Al and Zr improves the charge retention in AB$_5$-type alloys.

State-of-the-art Ni–MH cells have a specific energy of 95 Wh kg^{-1} and a volumetric energy density of 330 Wh l^{-1}. The specific power of the cells is 200 W kg^{-1} and the power density is 485 W l^{-1}. State-of-the-art metal hydride electrodes are prepared from transition metal alloys with a non-traditional structure design which deliver a capacity of 550–650 Ah kg^{-1}. Foam nickel with 90–95% porosity is used as the substrate for the positive electrode. The positive active material is based on an α to γ transformation as against the β to β transformation in conventional Ni–Cd cells.
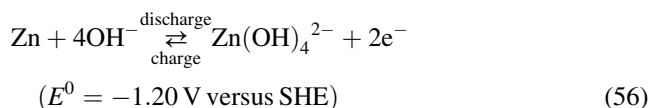
A very common problem with hydrogen storage materials is severe volume expansion during the charge–discharge process giving rise to cracking and pulverisation of the alloy making it amenable to oxidation. In addition, dissolution of the alloy in the electrolyte contributes to capacity decay. Present materials science strategies are concentrated on combining different phases and microstructures to overcome the short comings in the behaviour of the bulk metal hydride. To increase rate capability, materials with high surface-area are produced by powder metallurgy, mechanical alloying, chemical or electrochemical etching. All the materials with

high surface-area invariably suffer from lower cycle-life due to increased oxidation of the surface. The MH electrodes are susceptible to wide spread cracking and irreversible oxidation which affect their cycle-life, stability and rate capability. Metallurgical processes such as encapsulation (electroless plating of copper and nickel), doping with palladium and cerium, rapid solidification, and macroalloying are found to have only limited success in reducing the rate of degradation. Pure LaNi$_5$ electrodes in contact with KOH vapour undergo brittle fracture during hydriding resulting in rapid decay of capacity with cycling. Cobalt addition with aluminium or silicon has been found to significantly improve the cycling behaviour of Ni–MH cells. Laboratories around the world, in an effort to improve the cycle-life and capacity of metal hydride cells, have exhausted nearly all the elements in the periodic table in preparing both AB$_2$ and AB$_5$ alloys.

The major problem with the metal hydride electrodes is that the function of the alloying elements either acting alone or in combination with other alloying elements cannot be predicted unambiguously. Conventional AB$_5$ and AB$_2$ alloys based on LaNi$_5$ and (Ti, Zr)Ni$_2$ have relatively low Coulombic capacity values between 300 and 450 Ah kg^{-1} and hence, the present day research focuses on alloys such as TiZrNi$_2$ and Mg$_2$Ni alloys as low cost, light weight and safer alternatives. In order to increase the energy density of the Ni–MH battery, it is mandatory to improve the performance of metal-hydride electrodes. With a combination of modifications in the alloy composition and new methods of electrode preparation, discharge capacities between 630 and 780 Ah kg^{-1} have been achieved at a discharge current density of 50 A kg^{-1} for Mg-based alloy (Mg$_{1.9}$Al$_{0.1}$Ni$_{0.8}$Co$_{0.1}$Mn$_{0.1}$) electrodes [53]. An amorphous structure appears to be central in achieving high discharge capacities. These encouraging results indicate that the kinetics of hydriding/de-hydriding reactions of Mg-based alloy electrodes can be greatly improved by ball-milling and chemical coating. Efforts are being directed towards maintaining particle-to-particle electrical contact by the use of polymer binders, compaction of porous nickel foam, surface plating as well as doping and compaction with conductive powders. The performance of the Ni–MH batteries has seen continuous improvements over the years since 1991 through a combination of approaches such as high density negative electrodes, thinner separators, upgraded positive electrodes and improved packaging efficiencies.

6. Nickel–zinc batteries

In the Ni–Zn battery, zinc electrodes operate on the following dissolution–precipitation reactions.

$$\text{Zn} + 4\text{OH}^- \underset{\text{charge}}{\overset{\text{discharge}}{\rightleftarrows}} \text{Zn(OH)}_4^{2-} + 2\text{e}^-$$

$$(E^0 = -1.20\,\text{V versus SHE}) \tag{56}$$

The following precipitation reaction occurs concomitantly:

$$Zn(OH)_4{}^{2-} \underset{charge}{\overset{discharge}{\rightleftarrows}} ZnO + 2OH^- + H_2O \qquad (57)$$

ZnO produced during reaction (57) has the tendency to dissolve in aqueous KOH. As described earlier, the charge–discharge reactions occurring at the nickel positive electrode in the battery are

$$2NiOOH + 2H_2O + 2e^- \underset{charge}{\overset{discharge}{\rightleftarrows}} 2Ni(OH)_2 + 2OH^-$$
$$(E^0 = 0.49 \text{ V versus SHE}) \qquad (58)$$
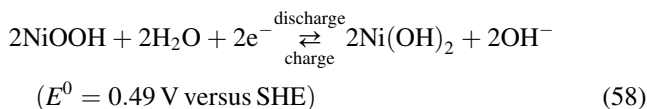
Accordingly, the overall cell discharge and charge reactions are expressed as

$$Zn + 2NiOOH + H_2O \underset{charge}{\overset{discharge}{\rightleftarrows}} ZnO + 2Ni(OH)_2$$
$$(E_{cell} = 1.75 \text{ V}) \qquad (59)$$
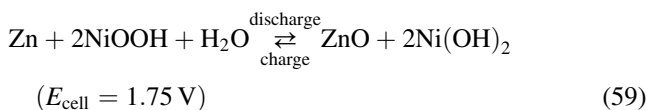
The electrolyte is usually 20–35 wt.% aqueous KOH with 1 wt.% LiOH which is saturated with ZnO. The LiOH addition enhances the charge acceptance of NiOOH electrode. Similarly, addition of NaOH to KOH has been found to extend the service life of Ni–Zn batteries while operating them at temperatures >50°C. The Ni–Zn battery is a promising alkaline storage battery and exhibits attractive performance with energy density values between 55 and 85 Wh kg^{-1}, power density values between 140 and 200 W kg^{-1}, and a self-discharge rate less than 0.8% per day. Besides, electrode materials used in the Ni–Zn batteries are abundant, and cost-effective. The batteries are produced in various configurations, namely vented static-electrolyte, sealed static-electrolyte, vibrating electrolyte and flowing electrolyte configurations [54–56]. Seminal features for these designs are briefly highlighted below.

Vented static-electrolyte nickel-zinc cells are designed to be positive-limited. While nickel positive electrodes are of the conventional sintered type formed either by an electrochemical or chemical precipitation process, the porous zinc negative electrode comprises a polymer-bonded paste of ZnO bonded to a current collecting mesh or screen. Calcium is a beneficial additive to the zinc electrode. When Ca(OH)$_2$ is added to ZnO in alkaline electrolyte, an insoluble calcium zincate compound is formed thereby 'trapping' the soluble Zn(OH)$_4{}^{2-}$ species. It has been found that both the active-mass ratio of the negative and positive plates and the zinc to electrolyte mass ratio in the Ni–Zn batteries critically affect the service life of the batteries. Various cell designs employ microporous separators to avoid the growth of zinc dendrites and wicking materials are used to help wetting the electrodes. These cells are vented to the atmosphere to allow the release of oxygen gas evolved during the charging process. The cells are held under compression to avoid the occurrence of any deformity during their service life. Sealed static-electrolyte Ni–Zn cells find applications that require low maintenance and safe operation. These batteries are akin to vented static electrolyte batteries in various design features, but the oxygen evolved at the nickel positive electrodes during the charging process is efficiently transferred to recombine at zinc electrode. In the vibrating-electrode Ni–Zn cells, a cam arrangement is used to vibrate the planar zinc electrode which agitates the electrolyte and results in uniform zincate-ion concentration which effectively eliminates the zinc active material redistribution problem. But owing to the complex mechanical components, such Ni–Zn batteries are no longer under production. In the flowing-electrolyte Ni–Zn batteries, zinc-coated polymer beads are circulated to the negative electrode compartment. These cells also are no longer under production.

After years of development and several patent awards, Ni–Zn batteries have achieved commercial viability. Present-day Ni–Zn batteries are in performance comparable with Ni–Cd and Ni–MH systems. The low material and manufacturing costs might make Ni–Zn batteries competitive even with the lead-acid batteries. Indeed, Ni–Zn battery technology has been licensed to several commercial entities for a variety of applications. A small scale manufacturing facility in the United States is currently producing commercial grade Ni–Zn batteries and a full-scale manufacturing joint-venture is coming online in China in the near-term.

7. Sodium–nickel chloride (zebra) batteries

In addition to the batteries described in the earlier sections, there is a high-temperature nickel-based battery in which the problem of dendritic-sodium growth in sodium–sulfur batteries has been cleverly circumvented with the use of sodium tetrachloro aluminate (NaAlCl$_4$) in conjunction with Na$^+$–β-alumina ceramic electrolyte. This battery was invented in 1985 by Coetzer in Pretoria (South Africa). Zebra stands for ZEolite applied to Battery Research Africa [57,58]. The battery operates at about 300°C and the charge–discharge reactions during the cell operation are as follows:

$$2Na + NiCl_2 \underset{charge}{\overset{discharge}{\rightleftarrows}} 2NaCl + Ni \qquad (E_{cell} = 2.58 \text{ V}) \quad (60)$$
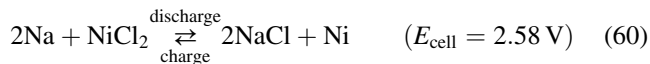
Since zebra batteries operate at ∼300°C, there are no detrimental effects resulting from their use at extremely cold or hot ambient temperatures. For conventional battery systems, extreme temperatures require more elaborate thermal management or result in reduced battery performance. Besides, because of their high-temperature operation, zebra batteries allow for the use of latent heat for fast cabin heating or window defrosting. But the thermal management needs for the high-temperature zebra batteries are not quite ideal for electric vehicle-drive-systems. When not in use, zebra batteries typically require being plugged into a wall plug, or tethered, in order to be ready for use when needed. If shut down, a reheating process must be initiated that requires about one to 2 days to restore the battery pack to the desired

temperature, and fully charging the batteries. This reheating time can, however, vary depending on the SOC of the batteries at the time of their shut down, battery-pack temperature, and power availed for reheating. If shut down of the battery pack is desired, three to 4 days are usually required for a fully-charged battery pack to lose its heat significantly. This battery is described in more details in the paper by Sudworth elsewhere in this volume.

8. Conclusions

Among the various nickel-based batteries reviewed above, Ni–MH batteries seem to have widespread commercial viability and significant opportunity for improvement. Ni–MH batteries appear to be the technology of choice for the emerging electric vehicles, hybrid electric vehicles and fuel cell electric vehicles. Important advances in positive and negative electrode materials have allowed, for the first time, prototype Ni–MH batteries of over 100 Wh kg^{-1} specific energy. At the same time, specific power has been increased from 150 to over 1000 W kg^{-1}, with further advances observed in the laboratory. Today, Ni–MH batteries occupy a unique position within the battery industry. Ni–MH batteries are rapidly growing and gaining an excellent reception in the market. Next generation improvements in Ni–MH batteries are already being implemented with still further improvements targeted.

References

[1] R.C. Weast, CRC Handbook of Chemistry and Physics, 57th Edition, CRC Press, Boca Raton, FL, 1976/1977, p. D-142.

[2] D.A. Corrigan, S.L. Knight, J. Electrochem. Soc. 136 (1989) 613.

[3] M. Dixit, R.S. Jayashree, P.V. Kamath, A.K. Shukla, V. Ganesh Kumar, N. Munichandraiah, Electrochem. Solid-State Lett. 2 (1999) 170.

[4] L.H. Thaller, A.H. Zimmerman, in: Proceedings of the 35th IECEC, Las Vegas, Navada, 24–28 July 2000, pp. 1073–1085.

[5] W. Ostwald, J. Phys. Chem. 22 (1897) 289.

[6] Y. Borthomieu, N. Sac-Epee, T. Jamin, in: Proceedings of the NASA Aerospace Battery Workshop, Huntsville, AL, 18–20 November 1997, pp. 587–626.

[7] S. Sathyanarayana, Trans. SAEST 11 (1976) 19–41.

[8] D. Berndt, Varta Special Report, July 1998.

[9] S.U. Falk, A.J. Salkind, Alkaline Storage Batteries, Electrochemical Society Series, Wiley, 1986.

[10] V.A. Ettel, NiCad'98, Prague, 21–22 September 1998.

[11] D. Linden, Handbook of Batteries and Fuel Cells, McGraw-Hill, New York, 1983.

[12] M. Cook, H. Morrow, Met. Bull., April (1992).

[13] S. Sathyanarayana, The Nickel–Iron Storage Batteries — A Status Report and Techno-Economic Survey for India, National Research Development Council, India, 1983.

[14] L. Ojefors, Studies on the Alkaline Iron-electrodes, Swedish National Development Co., Royal Institute of Technology, Stockholm, 1975.

[15] K. Vijayamohanan, T.S. Balasubramanian, A.K. Shukla, J. Power Sources 34 (1991) 269.

[16] S.U. Falk, A.J. Salkind, Alkaline Storage Batteries, Wiely, New York, 1969.

[17] O. Lindström, in: D.H. Collins (Ed.), Power Sources, Vol. 5, Academic Press, London, 1975, p. 283.

[18] J. Labat, J.C. Jarrousseau, J.F. Laurent, in: D.H. Collins (Ed.), Power Sources, Vol. 3, Oriel Press, Newcastle, UK, 1970, p. 283.

[19] K. Micka, Z. Zabransky, J. Power Sources 19 (1987) 315.

[20] L. Ojefors, J. Electrochem. Soc. 123 (1976) 1139.

[21] R.D. Armstrrong, I. Baurhoo, J. Electroanal. Chem. 34 (1972) 41.

[22] I.A. Ammar, Corros. Sci. 17 (1977) 583.

[23] T.S. Balasubramanian, K. Vijayamohanan, A.K. Shukla, J. Appl. Electrochem. 23 (1993) 947.

[24] T.S. Balasubramanian, Ph.D. Thesis, Indian Institute of Science, Bangalore, 1994.

[25] Environmental Aspects of Battery and Fuel Cell Technologies, UK Department of Trade and Industry Report, 1992, p. 11.

[26] K. Vijayamohanan, A.K. Shukla, S. Sathyanarayana, J. Electroanal. Chem. 289 (1990) 55.

[27] T.S. Balasubramanian, A.K. Shukla, J. Power Sources 41 (1993) 99.

[28] B. Hariprakash, P. Bera, S.K. Martha, S.A. Gaffoor, M.S. Hegde, A.K. Shukla, Electrochem. Solid-State Lett. 4 (3) (2001) A23.

[29] M.E. Unates, E. Folquer, J.R. Vilche, A.J. Arvia, J. Electrochem. Soc. 139 (1992) 2697–2704.

[30] E.J. Casey, A.R. Dubois, P.E. Lake, W.J. Moroz, J. Electrochem. Soc. 112 (1965) 371.

[31] A. Kozawa, A. Sato, ITE Battery Newsletter 1 (1996) 36.

[32] P. Scardaville, B. McRae, IEEE AES Systems Magazine, December 2000, pp. 11–14.

[33] M. Ikoma, Y. Hoshina, I. Masumoto, C. Iwakura, J. Electrochem. Soc. 143 (1996) 1904–1907.

[34] J.D. Dunlop, G.M. Rao, T.Y. Yi, NASA Handbook for Nickel–Hydrogen Batteries, NASA RP 1314, September 1993.

[35] D.F. Pickett, in: Proceedings of the 25th IECEC, Dayton, Ohio, 23–26 April 1990, Paper no. 901055.

[36] D.K. Coates, R.D. Wright, R.S. Repplinger, in: Proceedings of the Space Electrochemical Research and Technology, 1996, pp. 53–56.

[37] D.B. Caldwell, C.L. Fox, Lee Miller, in: Proceedings of the NASA Aerospace Battery Workshop, February 1997, pp. 405–411.

[38] V. Ganesh Kumar, Ph.D. Thesis, Indian Institute of Science, Bangalore, 1999.

[39] G. Sandrock, in: P.D. Bennett, T. Sakai (Eds.), Hydrogen and Metal Hydride Batteries, PV 94-27, in: Proceedings of the Electrochemical Society Series, Pennington, NJ, 1994.

[40] E.W. Justi, H.H. Ewe, A.W. Kalberlah, N.M. Saridakis, M.H. Schaefer, Energy Conversion 10 (1970) 183.

[41] G. Bronoel, J. Sarradin, M. Bonnemony, A. Percheron, J.C. Achard, L. Schlapbach, Int. J. Hydrogen Energy 1 (1976) 251.

[42] H. Büchner, Energiespeicherung in Metallhydriden, Springer, Vienna, 1982, p. 211.

[43] A.P. Guegan, J.C. Achard, J. Sarradin, G. Bronoel, in: A.F. Andresen, A.J. Maeland (Eds.), Hydride for Energy Storage, Pergamon, Oxford, 1978, p. 485.

[44] J.J.G. Willems, Philips J. Res. 39 (1984) 1.

[45] S.R. Ovshinsky, Material Research Society Meeting, Boston, MA, 30 November–4 December 1998.

[46] N. Furukawa, J. Power Sources 51 (1994) 45.

[47] S.R. Ovshinsky, M.A. Fetcenko, S. Venkatesan, B. Chao, Disordered Materials in Consumer and Electric Vehicle Nickel–Metal Hydride Batteries, San Francisco, CA, 1994.

[48] S.R. Ovshinsky, M.A. Fetcenko, J. Ross, Science 260 (1993) 176.

[49] T. Kohno, M. Yamamoto, M. Kanda, J. Alloys Comp. 193–295 (1999) 643–647.

[50] S.R. Ovshinsky, S.K. Dhar, M.A. Fetcenko, D.A. Corrigan, B. Reichman, K. Yong, C. Fierro, S. Venkatesan, P. Giffordand, J. Koch, in: Proceedings of the 14th International Seminar on Primary and Secondary Batteries, Ft. Lauderdale, Florida, 3 March 1988.

[51] N. Cui, J.L. Luo, K.T. Chuang, J. Alloys Comp. 302 (2000) 18–26.

[52] N. Kuriyama, T. Sakai, H. Miyamura, A. Kato, H. Ishikawa, Solid-State Ionics 40/41 (1990) 906.

[53] L. Sun, H.K. Liu, D. Bradhurst, S.X. Dou, Electrochem. Solid-State Lett. 2 (1999) 164.

[54] J. Jindra, J. Power Sources 66 (1997) 15.

[55] F.R. McLarnon, E.J. Cairns, J. Electrochem. Soc. 138 (1991) 645.

[56] J. McBreen, J. Power Sources 51 (1994) 37.

[57] D.A.J. Rand, R. Woods, R.M. Dell, Batteries for Electric Vehicles, Research Studies Press, England, 1998.

[58] J.L. Sudworth, J. Power Sources 51 (1994) 105.